Three Problems in Unconventional Coordinates Systems

(Conduction in a spheroid, Flow in a semi-elliptic tube, Conduction from a torus)

BY

Mohammed Ahmed AbuShoshah

A Thesis Presented to the

DEANSHIP OF GRADUATE STUDIES

KING FAHD UNIVERSITY OF PETROLEUM & MINERALS

DHAHRAN, SAUDI ARABIA

In Partial Fulfillment of the
Requirements for the Degree of

MASTER OF SCIENCE

In

Mathematics

April, 2013

KING FAHD UNIVERSITY OF PETROLEUM & MINERALS

DHAHRAN- 31261, SAUDI ARABIA

DEANSHIP OF GRADUATE STUDIES

This thesis, written by **Mohammed Ahmed AbuShoshah** under the direction his thesis advisor and approved by his thesis committee, has been presented and accepted by the Dean of Graduate Studies, in partial fulfillment of the requirements for the degree of **MASTER OF SCIENCE IN MATHEMATICS.**

Dr. Rajai Alassar
(Advisor)

Dr. Hattan Tawfiq
Department Chairman

Dr. Mohammed El-Gebeily
(Co-Advisor)

Dr. Salam A. Zummo
Dean of Graduate Studies

Dr. Tahir Mustafa
(Member)

6/5/13
Date

Dr. Salim Messaoudi
(Member)

Dr. Usamah Al-Mubaiyedh
(Member)

To my mother..

May Allah grant her a place in Jannat Al-Firdous

ACKNOWLEDGMENTS

First and foremost, my profound gratitude is to almighty Allah, the most compassionate and the most merciful, for his countless blessings.

I am particularly thankful to my Advisor, **Prof. Rajai Alassar**. I must confess that this work fruited due to his effort, his time, his patience against all my shortcomings and his attitude in encouraging, advising and supporting me in writing this work. Because of his high quality directions, and friendly relationship, this work has seen light. I am really proud to have had him as my committee advisor, and I will be grateful to him forever.

I am deeply thankful to my committee members for their support and advices. My appreciation is due to the Department of Math and Stat at King Fahd University of Petroleum and Minerals (KFUPM) for providing such a nice environment that made this research possible.

I am highly indebted to my family; my father, and my sisters and brothers. Lastly, but not the least, any worthy achievement has surely been shared by my beloved wife.

TABLE OF CONTENTS

LIST OF TABLES

LIST OF FIGURES

CHAPTER 1: Curl and Divergence Operators for General Coordinates Systems

CHAPTER 2: Heat Conduction in a Spheroid

CHAPTER 3: Hagen-Poiseuille Flow in a Semi-Elliptic Tube

CHAPTER 4: Heat Conduction from a Tours

ABSTRACT

Full Name : Mohammed Ahmed AbuShoshah
Thesis Title : Three Problems in Unconventional Coordinates Systems
(Conduction in a spheroid, Flow in a semi-elliptic tube, Conduction from a torus)
Major Field : Mathematics
Date of Degree : April, 2013

In this research, simple generalized expressions for the curl and divergence operators for any coordinates system, not necessarily orthogonal, are obtained. These expressions appear in differential equations which model several physical systems.

In particular, solutions of the following three problems, described in their appropriate coordinates systems, are attempted:

1. Heat conduction in a spheroid
2. Hagen-Poiseuille flow in a tube of semi-elliptic cross section
3. Heat conduction from a torus

ملخص الرسالة

الاسم الكامل: محمد بن أحمد بن إبراهيم أبوشوشة

عنوان الرسالة: ثلاث مسائل في أنظمة محاور غير اعتيادية (انتقال الحرارة في جسم شبه كروي، تدفق في أنابيب ذات مقطع نصف بيضاوي، انتقال الحرارة من جسم حلقي)

التخصص: علم الرياضيات

تاريخ الدرجة العلمية: جمادى الآخر، ١٤٣٤هـ

نحصلُ في هذا البحث على عباراتٍ رياضية عامة وبسيطة لمؤثريْ الدوران والتباعد لأي نظام محاور، ليس متعامداً بالضرورة. تعتبر هذه العبارات مكوِّناً أساسياً للمعادلات التفاضلية التي تصف العديد من الأنظمة الطبيعية. وعلى وجه الخصوص، نحصل على حلول للمسائل الثلاثة التالية باستخدام أنظمة محاورها المناسبة:

١. انتقال الحرارة بالتوصيل في جسم شبه كروي
٢. تدفق "هاجن بوسيل" في الأنابيب ذات المقاطع نصف البيضاوية
٣. انتقال الحرارة بالتوصيل من جسم حلقي

CHAPTER 1: Curl and Divergence Operators for General Coordinates Systems

1.1 Introduction

The curl and divergence operators play significant roles in physical relations. They arise in fluid mechanics, elasticity theory and are fundamental in the theory of electromagnetism.

The physical significance of the **Curl** of a vector field $\vec{F}$, denoted by $\vec{\nabla}\times\vec{F}$, is that it measures the amount of rotation or angular momentum of the contents of a given region of space. If the value of the curl is zero then the field is said to be irrotational The curl is defined in an arbitrary ***orthogonal*** curvilinear coordinates (u_1, u_2, u_3) as

$$\vec{\nabla}\times\vec{F} = \frac{1}{h_1 h_2 h_3}\begin{vmatrix} h_1\boldsymbol{e_1} & h_2\boldsymbol{e_2} & h_3\boldsymbol{e_3} \\ \dfrac{\partial}{\partial u_1} & \dfrac{\partial}{\partial u_2} & \dfrac{\partial}{\partial u_3} \\ \mathrm{F}_1 h_1 & \mathrm{F}_2 h_2 & \mathrm{F}_3 h_3 \end{vmatrix} \tag{1}$$

where $\boldsymbol{e_i}$ is a unit vector in the direction of u_i, and $\vec{F} = F_1\boldsymbol{e_1} + F_2\boldsymbol{e_2} + F_3\boldsymbol{e_3}$. The length of the tangent vector in the direction of u_i is known as the scale factor, h_i, and is defined by

$$h_i = \left|\frac{\partial\vec{r}}{\partial u_i}\right| \tag{2}$$

where $\vec{r}$ is the position vector in any three dimensional space, i.e. $\vec{r} = \vec{r}(u_1, u_2, u_3)$, $\dfrac{\partial \vec{r}}{\partial u_i}$ is a tangent vector to the u_i curve where the other two coordinates variables remain constant. A unit tangent vector in this direction, therefore, is

$$\boldsymbol{e_i} = \frac{\dfrac{\partial \vec{r}}{\partial u_i}}{\left|\dfrac{\partial \vec{r}}{\partial u_i}\right|} = \frac{\dfrac{\partial \vec{r}}{\partial u_i}}{h_i} \qquad \text{or} \qquad \frac{\partial \vec{r}}{\partial u_i} = h_i \boldsymbol{e_i} \tag{3}$$

The **Divergence** of a vector field over a control volume V bounded by the surface S, denoted by $\vec{\nabla} \bullet \vec{F}$, is defined by

$$\vec{\nabla} \bullet \vec{F} = \lim_{V \to 0} \frac{\oint_S \vec{F} \bullet \vec{n}\, dS}{V} \tag{4}$$

where $\vec{n}$ is an outward unit normal vector to the surface S. The divergence actually measures the net outflow of a vector field from an infinitesimal volume around a given point (or how much a vector field "converges to" or "diverges from" a given point). The general expression of the divergence for arbitrary ***orthogonal*** curvilinear coordinates is given by

$$\vec{\nabla} \bullet \vec{F} = \frac{1}{h_1 h_2 h_3}\left[\frac{\partial}{\partial u_1}(F_1 h_2 h_3) + \frac{\partial}{\partial u_2}(F_2 h_1 h_3) + \frac{\partial}{\partial u_3}(F_3 h_1 h_2)\right] \tag{5}$$

The **Laplacian** operator of a scalar $\psi = \psi(u_1, u_2, u_3)$, denoted by $\nabla^2 \psi$ is defined as the divergence of the gradient of ψ; that is

$$\nabla^2\psi = \vec{\nabla}\bullet(\vec{\nabla}\psi) = \frac{1}{h_1 h_2 h_3}\left[\frac{\partial}{\partial u_1}\left(\frac{h_2 h_3}{h_1}\frac{\partial\psi}{\partial \mathrm{u}_1}\right)+\frac{\partial}{\partial u_2}\left(\frac{h_1 h_3}{h_2}\frac{\partial\psi}{\partial u_2}\right)+\frac{\partial}{\partial u_3}\left(\frac{h_1 h_2}{h_3}\frac{\partial\psi}{\partial u_3}\right)\right] \qquad (6)$$

where $\vec{\nabla}\psi = \frac{1}{h_1}\frac{\partial\psi}{\partial u_1}\boldsymbol{e_1}+\frac{1}{h_2}\frac{\partial\psi}{\partial u_2}\boldsymbol{e}_2+\frac{1}{h_3}\frac{\partial\psi}{\partial u_3}\boldsymbol{e}_3$ (7)

Equations (1), (5), and (6) are valid for ***orthogonal*** systems only (i.e. $\boldsymbol{e_1}$, $\boldsymbol{e}_2$, and $\boldsymbol{e}_3$ are orthogonal), [1, 2, 3]. An attempt is made here to derive simple generalized expressions for general coordinates systems, whether orthogonal or not, as such expressions are required in several physical situations.

1.2 Divergence for General Coordinates Systems

The **Divergence Theorem** relates the net flux of a vector field through a surface to the divergence of the vector field. More precisely, it states that the net outward flux of a vector field through a closed surface is equal to the volume integral of the divergence over the region inside the surface, i.e.

$$\iint_S \vec{w}\bullet\vec{n}\,dS = \iiint_D \vec{\nabla}\bullet\vec{w}\,dv \qquad (8)$$

where

D is a closed bounded region with piecewise smooth boundary *S*, $\vec{n}$ is an outer unit vector normal to the surface *S*, $\vec{w} = w_1\boldsymbol{e_1} + w_2\boldsymbol{e_2} + w_3\boldsymbol{e}_3$, $\vec{w}\bullet\vec{n}$ represents the component of $\vec{w}$ in the direction of $\vec{n}$, and dv is the volume of the region *D*.

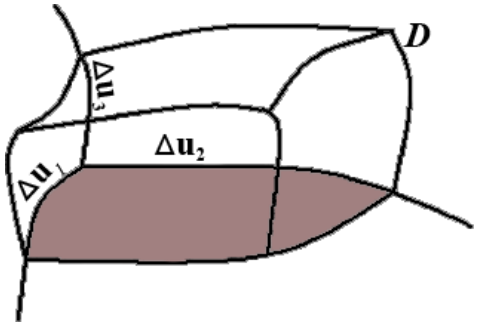

Figure 1: An infinitesimal control volume

Considering the bottom shaded surface dS of the given control volume, **Figure 1**, one can find that

$$\vec{n} = -\frac{\dfrac{\partial \vec{r}}{\partial u_1} \times \dfrac{\partial \vec{r}}{\partial u_2}}{\left| \dfrac{\partial \vec{r}}{\partial u_1} \times \dfrac{\partial \vec{r}}{\partial u_2} \right|}, \quad \text{and} \quad dS = \left| \frac{\partial \vec{r}}{\partial u_1} \times \frac{\partial \vec{r}}{\partial u_2} \right| du_1 du_2.$$

Hence

$$\begin{aligned} \vec{w} \bullet \vec{n}\, dS &= -\vec{w} \bullet \frac{\dfrac{\partial \vec{r}}{\partial u_1} \times \dfrac{\partial \vec{r}}{\partial u_2}}{\left| \dfrac{\partial \vec{r}}{\partial u_1} \times \dfrac{\partial \vec{r}}{\partial u_2} \right|} \left| \frac{\partial \vec{r}}{\partial u_1} \times \frac{\partial \vec{r}}{\partial u_2} \right| du_1 du_2 \\ &= -(w_1 \boldsymbol{e_1} + w_2 \boldsymbol{e_2} + w_3 \boldsymbol{e_3}) \bullet \left(h_1 \boldsymbol{e_1} \times h_2 \boldsymbol{e_2} \right) du_1 du_2 \\ &= -w_3 \left(\boldsymbol{e_3} \bullet \boldsymbol{e_1} \times \boldsymbol{e_2} \right) h_1 h_2 \, du_1 du_2 \end{aligned}$$

On the upper surface, using Taylor series, the outward flux is

$$w_3 \left(\boldsymbol{e_3} \bullet \boldsymbol{e_1} \times \boldsymbol{e_2} \right) h_1 h_2 du_1 du_2 + \frac{\partial}{\partial u_3} \left[w_3 \left(\boldsymbol{e_3} \bullet \boldsymbol{e_1} \times \boldsymbol{e_2} \right) h_1 h_2 \right] du_1 du_2 du_3 + \cdots$$

The net flux through the upper and lower surfaces, then, is

$$\frac{\partial}{\partial u_3} \left[\left(\boldsymbol{e_3} \bullet \boldsymbol{e_1} \times \boldsymbol{e_2} \right) w_3 h_1 h_2 \right] du_1 du_2 du_3 + \cdots \tag{9}$$

Using the same argument, the net flux through the remaining two pairs of surfaces are:

$$\frac{\partial}{\partial u_2}\left[\left(\boldsymbol{e_3}\bullet\boldsymbol{e_1}\times\boldsymbol{e_2}\right)w_2h_1h_3\right]du_1du_2du_3+\cdots \tag{10}$$

$$\frac{\partial}{\partial u_1}\left[\left(\boldsymbol{e_3}\bullet\boldsymbol{e_1}\times\boldsymbol{e_2}\right)w_1h_2h_3\right]du_1du_2du_3+\cdots \tag{11}$$

$\vec{w}\bullet\vec{n}\,dS$ on the left hand side of equation (8) becomes

$$\left(\frac{\partial}{\partial u_3}\left[ew_3h_1h_2\right]+\frac{\partial}{\partial u_2}\left[ew_2h_1h_3\right]+\frac{\partial}{\partial u_1}\left[ew_1h_2h_3\right]\right)du_1du_2du_3+\cdots \tag{12}$$

where $e=\boldsymbol{e_3}\bullet\boldsymbol{e_1}\times\boldsymbol{e_2}$ is an orthognality indicator of the system, $\left(0<e\le 1\right)$.

The volume element, dv, is given by

$$dv=\left(h_3\boldsymbol{e_3}\,du_3\right)\bullet\left(h_1\boldsymbol{e_1}\,du_1\times h_2\boldsymbol{e_2}\,du_2\right) \tag{13}$$

The right hand side of equation (8), then, is

$$\begin{aligned}\vec{\nabla}\bullet\vec{w}\,dv&=\vec{\nabla}\bullet\vec{w}\left(h_3\boldsymbol{e_3}\,du_3\right)\bullet\left(h_1\boldsymbol{e_1}\,du_1\times h_2\boldsymbol{e_2}\,du_2\right)\\&=\vec{\nabla}\bullet\vec{w}\left(\boldsymbol{e_3}\bullet\boldsymbol{e_1}\times\boldsymbol{e_2}\right)\left(h_1h_2h_3du_1du_2du_3\right)\\&=\vec{\nabla}\bullet\vec{w}\,e\left(h_1h_2h_3\,du_1du_2du_3\right)\end{aligned} \tag{14}$$

In the limit, by equating (12) and (14), an expression for the divergence of a vector field $\vec{w}$ in a general coordinates system, whether orthogonal or not, is given by

$$\vec{\nabla}\bullet\vec{w}=\frac{1}{e\,h_1h_2h_3}\left(\frac{\partial}{\partial u_3}\left[e\,w_3h_1h_2\right]+\frac{\partial}{\partial u_2}\left[e\,w_2h_1h_3\right]+\frac{\partial}{\partial u_1}\left[e\,w_1h_2h_3\right]\right) \tag{15}$$

It is easy to see that when $e=1$ (orthogonal system), equation (15) reduces to (5).

1.3 Curl for General Coordinates Systems

Stokes' Theorem relates the surface integral of the curl of a vector field over a surface to the line integral of the vector field over the surface boundary, or

$$\iint_S \vec{\nabla}\times\vec{w}\bullet\vec{n}\ dS = \oint_c \vec{w}\bullet dr \tag{16}$$

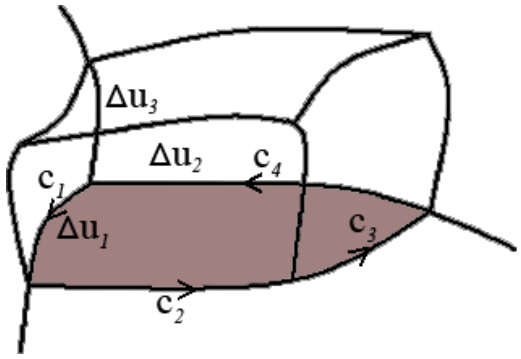

Figure 2: An infinitesimal surface enclosed by the closed path *c*

Considering the bottom shaded surface of the given control volume, **Figure 2**,

$$\begin{aligned}\vec{\nabla}\times\vec{w}\bullet\vec{n}\,dS &= \left((\vec{\nabla}\times\vec{w})_1\boldsymbol{e}_1+(\vec{\nabla}\times\vec{w})_2\boldsymbol{e}_2+(\vec{\nabla}\times\vec{w})_3\boldsymbol{e}_3\right)\bullet\left(\frac{h_1\boldsymbol{e}_1\times h_2\boldsymbol{e}_2}{|h_1\boldsymbol{e}_1\times h_2\boldsymbol{e}_2|}\right)|h_1\boldsymbol{e}_1\times h_2\boldsymbol{e}_2|\,du_1du_2\\ &= \left((\vec{\nabla}\times\vec{w})_3\boldsymbol{e}_3\right)\bullet\left(\boldsymbol{e}_1\times\boldsymbol{e}_2\right)h_1h_2\,du_1\,du_2\\ &= (\vec{\nabla}\times\vec{w})_3\,e\,h_1h_2du_1du_2\end{aligned} \tag{17}$$

where $(\vec{\nabla}\times\vec{w})_i$ is the component of $\vec{\nabla}\times\vec{w}$ in the direction of $\boldsymbol{e}_i$.

$\vec{w}\bullet dr$ in equation (16), over the four segments comprising the curve *c*, is

$$\begin{aligned}\vec{w}\bullet dr &= \vec{w}\bullet dr\big|_{c1}+\vec{w}\bullet dr\big|_{c2}+\vec{w}\bullet dr\big|_{c3}+\vec{w}\bullet dr\big|_{c4}\\ &= \vec{w}\bullet dr\big|_{c1}+\vec{w}\bullet dr\big|_{c3}+\vec{w}\bullet dr\big|_{c4}+\vec{w}\bullet dr\big|_{c2}\end{aligned}$$

$$= (\vec{w} \bullet h_1 \boldsymbol{e}_1 du_1) + \left(-\vec{w} \bullet h_1 \boldsymbol{e}_1 du_1 + \frac{\partial}{\partial u_2} \left[-\vec{w} \bullet h_1 \boldsymbol{e}_1 du_1 \right] du_2 \right) + \cdots$$

$$+ (-\vec{w} \bullet h_2 \boldsymbol{e}_2 du_2) + \left(\vec{w} \bullet h_2 \boldsymbol{e}_2 du_2 + \frac{\partial}{\partial u_1} \left[\vec{w} \bullet h_2 \boldsymbol{e}_2 du_2 \right] du_1 \right) + \cdots$$

or

$$\vec{w} \bullet d\boldsymbol{r} = \left(\frac{\partial}{\partial u_1} \left[\vec{w} \bullet h_2 \boldsymbol{e}_2 \right] - \frac{\partial}{\partial u_2} \left[\vec{w} \bullet h_1 \boldsymbol{e}_1 \right] \right) du_1 du_2 + \cdots \tag{18}$$

In the limit, after equating (17) and (18),

$$(\vec{\nabla} \times \vec{w})_3 = \frac{1}{e\, h_1 h_2} \left(\frac{\partial}{\partial u_1} [h_2 \vec{w} \bullet \boldsymbol{e}_2] - \frac{\partial}{\partial u_2} [h_1 \vec{w} \bullet \boldsymbol{e}_1] \right) \tag{19}$$

Similar results can be obtained for the other two surfaces shown in **Figure 3**.

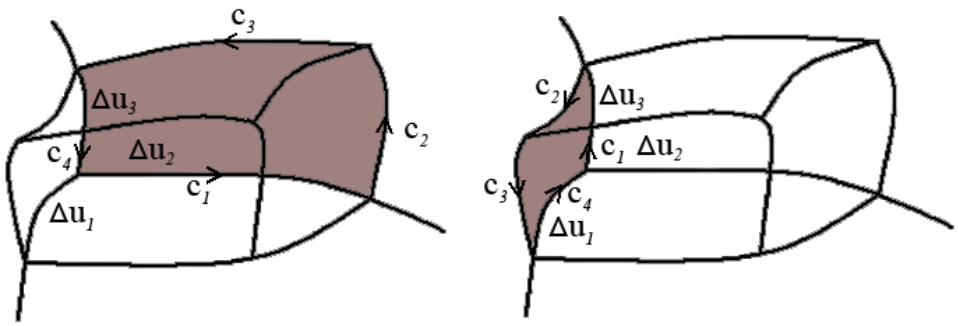

Figure 3: Two infinitesimal surfaces enclosed by the closed path *c*

$$(\vec{\nabla} \times \vec{w})_2 = \frac{1}{e\, h_3 h_1} \left(\frac{\partial}{\partial u_3} [h_1 \vec{w} \bullet \boldsymbol{e}_1] - \frac{\partial}{\partial u_1} [h_3 \vec{w} \bullet \boldsymbol{e}_3] \right) \tag{20}$$

$$(\vec{\nabla} \times \vec{w})_1 = \frac{1}{e\, h_3 h_2} \left(\frac{\partial}{\partial u_2} [h_3 \vec{w} \bullet \boldsymbol{e}_3] - \frac{\partial}{\partial u_3} [h_2 \vec{w} \bullet \boldsymbol{e}_2] \right) \tag{21}$$

Equations (19), (20) and (21) can be written in the concise form

$$\vec{\nabla}\times\vec{w} = \frac{1}{e\, h_1 h_2 h_3}\begin{vmatrix} h_1\boldsymbol{e}_1 & h_2\boldsymbol{e}_2 & h_3\boldsymbol{e}_3 \\ \dfrac{\partial}{\partial u_1} & \dfrac{\partial}{\partial u_2} & \dfrac{\partial}{\partial u_3} \\ h_1\vec{w}\bullet\boldsymbol{e}_1 & h_2\vec{w}\bullet\boldsymbol{e}_2 & h_3\vec{w}\bullet\boldsymbol{e}_3 \end{vmatrix} \tag{22}$$

Obviously, the difference between orthogonal and nonorthogonal coordinates systems lies in the introduction of the scalar triple product $e = \boldsymbol{e}_3 \bullet \boldsymbol{e}_1 \times \boldsymbol{e}_2$ into the expressions of $\vec{\nabla}\times\vec{F}$, and $\vec{\nabla}\bullet\vec{F}$. This product returns a value of unity if the coordinates system is orthogonal and vanishes for two-dimensional systems.

CHAPTER 2: Heat Conduction in a Spheroid

2.1 Introduction

The problem of heat transfer from spherical or spheroidal particles is important due to the related applications. A spheroid represents more realistic situations not observed in the idealization of particles through spheres. A sphere is, in fact, a special case of the generalized spheroidal geometry. The study is interesting from academic as well as practical viewpoints. For example, most aerosols are not spherical in nature, Williams [4]. The solution of the problem under consideration also has relevance in heat transfer in stationary packed beds and drying processes. Generally, the results of the present research are of use to a wide range of applications where Biot and Rayleigh numbers are high and fluid heat conduction dominates the thermal resistance. Such conditions can be found at small length scales.

The problem of heat conduction from spheroids dates back to Niven [5] who presented an excellent theoretical treatment. Niven's work, in terms of spheroidal wave functions, must have been confronted with the limited computation powers at that time. Attempts to establish a theoretical and calculational backbone for the spheroidal wave functions have not stopped since then. These include the distinguished work of Falloon et al. [6], Flammer [7], Abramowitz and Stegun [8], Stratton [9], Meixner et al. [10], Caldwell [11], Hodge [12], Baker [13], Li et al. [14], and Zayed [15]. A more recent study that deals with heat transfer from a spheroid has been carried out by Ivers [16]. Again, apart from the theoretical aspects of the problem, one spots no analysis or actual treatment of

the conduction process. The related steady states heat conduction problem to an infinite medium was carried by Alassar [17]. The problem is different from the one under investigation in that it deals with the steady states version outside a spheroid of constant temperature.

2.2 Problem Statement

We consider the problem of heat conduction in a spheroid. The spheroid, prolate or oblate, has major and minor axes of length 2*a* and 2*b*, respectively, with $c = \sqrt{a^2 - b^2}$ being the focal distance, **Figure 4**, [1, 2, 3]. The spheroid is heated to a uniform temperature T_0 and then left to cool in an infinite medium of constant temperature, T_∞.

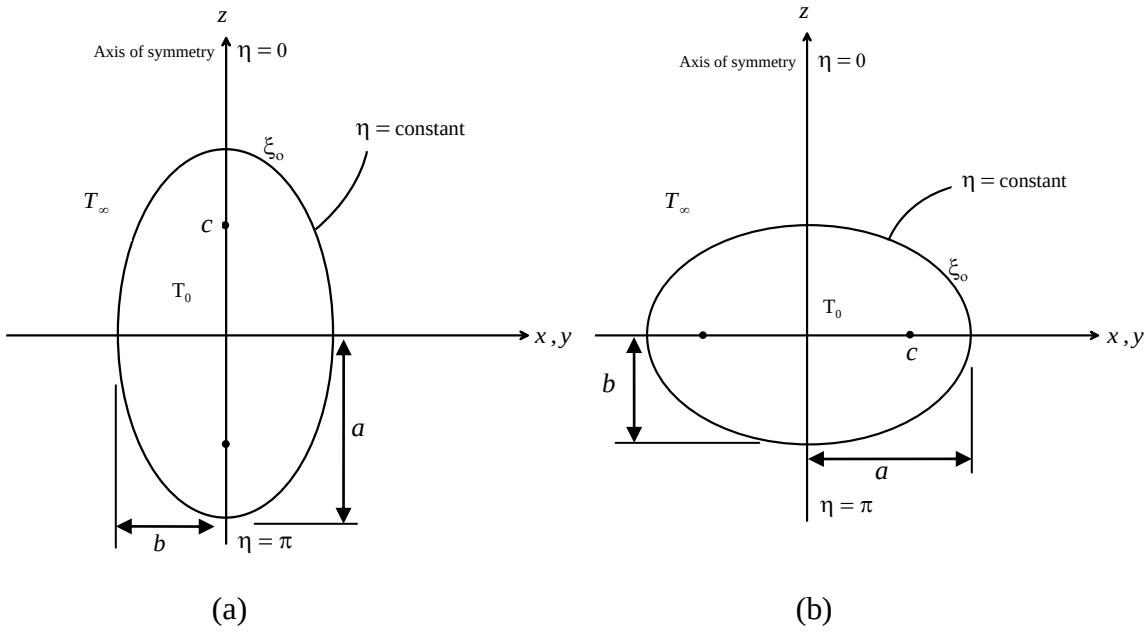

Figure 4: Problem configuration; (a)Prolate, (b)Oblate

2.3 Prolate and Oblate Spheroidal Coordinates

The proper coordinates systems that coincide with the boundary surfaces of the regions in the present problem are the prolate and oblate spheroidal coordinates (ξ, η, φ). The prolate spheroidal coordinates system, **Figure 5**, is generated by rotating an ellipse around its major axis. It is related to the cartesian coordinates systems by

$$\begin{aligned} x &= c\ \sinh\xi\ \sin\eta\ \cos\varphi \\ y &= c\ \sinh\xi\ \sin\eta\ \sin\varphi \\ z &= c\ \cosh\xi\ \cos\eta \end{aligned} \tag{23}$$

where $(0 \le \xi < \infty)$, $(0 \le \eta \le \pi)$, and $(0 \le \varphi < 2\pi)$.

The corresponding scale factors are

$$h_\xi = h_\eta = c\sqrt{\sinh^2\xi + \sin^2\eta}, \qquad h_\varphi = c\ \sinh\xi\ \sin\eta \tag{24}$$

The prolate spheroidal coordinates has the following coordinate surfaces:

- Prolate spheroids, (ξ = constant),

$$\frac{x^2}{c^2\sinh^2\xi} + \frac{y^2}{c^2\sinh^2\xi} + \frac{z^2}{c^2\cosh^2\xi} = 1$$

- Hyperboloids of two sheets, (η = constant),

$$\frac{z^2}{c^2\cos^2\eta} - \frac{x^2}{c^2\sin^2\eta} - \frac{y^2}{c^2\sin^2\eta} = 1$$

- Half planes through the *z*-axis, (φ = constant),

$$y = x\ \tan\varphi$$

An infinitesimal volume element in prolate spheroidal coordinates system is given by

$$dV = h_\xi h_\eta h_\varphi d\xi d\eta d\varphi = c^3\left(\sinh^3\xi\sin\eta + \sinh\xi\sin^3\eta\right) d\xi d\eta d\varphi \tag{25}$$

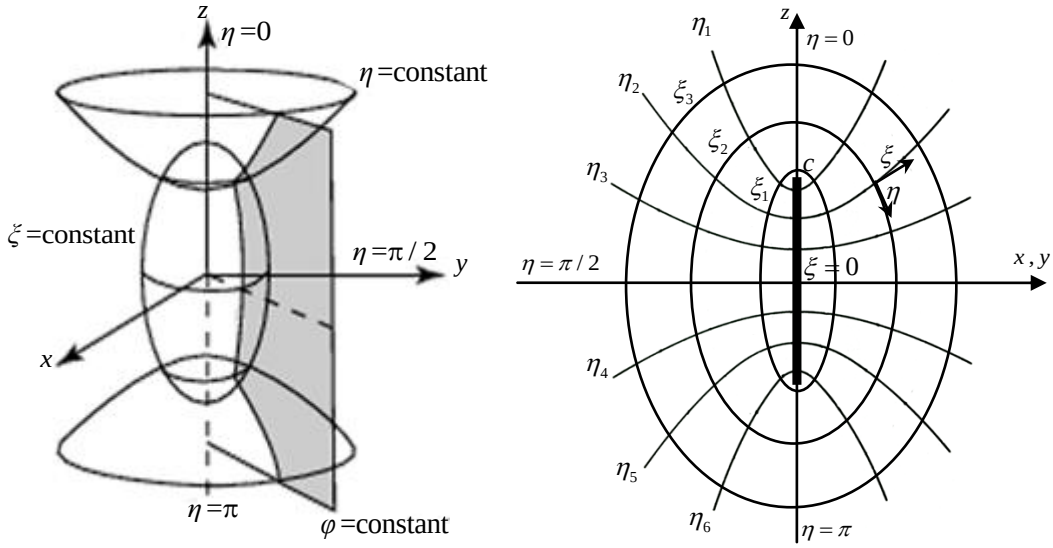

Figure 5: Prolate Spheroidal Coordinates, [1,29]

On the other hand, the oblate spheroidal coordinates system, **Figure 6**, is generated by rotating an ellipse around its minor axis, **Figure 4**. This system is related to the cartesian coordinate by

$$\begin{aligned} x &= c\ \cosh\xi\ \sin\eta\ \cos\phi \\ y &= c\ \cosh\xi\ \sin\eta\ \sin\phi \\ z &= c\ \sinh\xi\ \cos\eta \end{aligned} \tag{26}$$

where $(0 \le \xi < \infty)$, $(0 \le \eta \le \pi)$, and $(0 \le \varphi < 2\pi)$.

the corresponding scale factors are:

$$h_\xi = h_\eta = c\sqrt{\sinh^2\xi + \cos^2\eta}, \qquad h_\phi = c\cosh\xi\sin\eta \tag{27}$$

The oblate spheroidal coordinates has the following coordinate surfaces:

- Oblate spheroids, (ξ = constant),

$$\frac{x^2}{c^2\cosh^2\xi}+\frac{y^2}{c^2\cosh^2\xi}+\frac{z^2}{c^2\sinh^2\xi}=1$$

- Hyperboloids of one sheet, (η = constant),

$$\frac{x^2}{c^2\sin^2\eta}+\frac{y^2}{c^2\sin^2\eta}-\frac{z^2}{c^2\cos^2\eta}=1$$

- Half planes through the z-axis, (φ = constant),

$$y = x\tan\varphi$$

An infinitesimal volume element in oblate spheroidal coordinates is given by

$$dV = h_\xi h_\eta h_\varphi d\xi\, d\eta\, d\varphi = c^3\left(\sinh^2\xi+\cos^2\eta\right)\cosh\xi\sin\eta\, d\xi\, d\eta\, d\varphi \qquad (28)$$

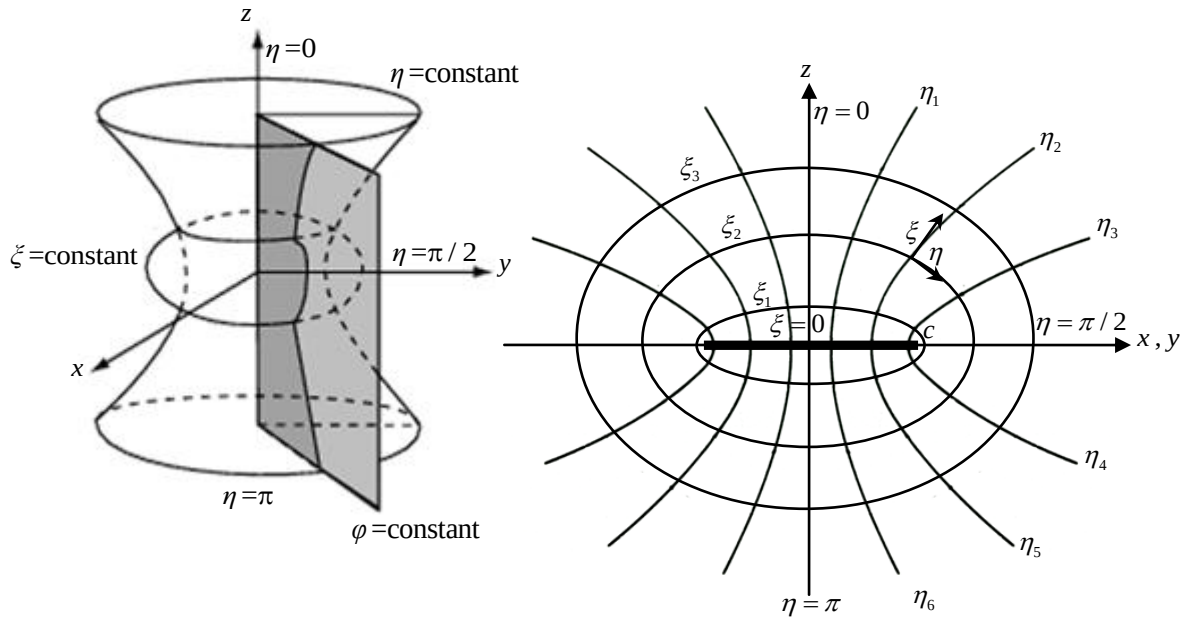

Figure 6: Oblate Spheroidal Coordinates, [1,29]

The surface of the spheroid, whether prolate or oblate, is defined by ξ_o which is related to the axis ratio *b/a* by

$$\xi_0 = \tanh^{-1}(b/a) \tag{29}$$

The limiting case for both coordinates, as ξ_o tends to infinity, is a sphere. On the other hand, as ξ_o tends to zero, the oblate spheroid becomes a flat circular disk while the prolate spheroid becomes an infinitely thin needle.

2.4 Governing Differential Equation and Boundary Conditions

For a homogeneous and isotropic medium with no heat generation, the energy equation can be written as

$$\nabla^2 T(\vec{r},t) = \frac{1}{\alpha}\frac{\partial T}{\partial t} \tag{30}$$

where T is the temperature, t is the time, $\alpha = \dfrac{K}{\rho C_p}$ is the thermal diffusivity, K is the thermal conductivity, ρ is the density of the material, and C_p is the specific heat.

Considering the obvious symmetry in the direction of φ, i.e. $T = T(\xi,\eta,t)$, the heat conduction equation, (30), can be specialized for prolate and oblate spheroidal coordinates, respectively, as

$$\frac{1}{c^2(\sinh^2\xi+\sin^2\eta)}\left[\frac{1}{\sin\eta}\frac{\partial}{\partial\eta}(\sin\eta\frac{\partial T}{\partial\eta})+\frac{1}{\sinh\xi}\frac{\partial}{\partial\xi}(\sinh\xi\frac{\partial T}{\partial\xi})\right]=\frac{1}{\alpha}\frac{\partial T}{\partial t} \tag{31}$$

$$\frac{1}{c^2(\sinh^2\xi+\cos^2\eta)}\left[\frac{1}{\sin\eta}\frac{\partial}{\partial\eta}(\sin\eta\frac{\partial T}{\partial\eta})+\frac{1}{\cosh\xi}\frac{\partial}{\partial\xi}(\cosh\xi\frac{\partial T}{\partial\xi})\right]=\frac{1}{\alpha}\frac{\partial T}{\partial t} \tag{32}$$

The first boundary condition, to be considered, is that the surface of the spheroid is maintained at the constant temperature of the infinite medium, while the second ensures that the solution remains bounded at $\xi = 0.$ These conditions can be written as

$$T(\eta, \xi_0, t) = T_\infty \qquad T(\eta, 0, t) < \infty \tag{33}$$

The initial condition is

$$T(\eta, \xi, 0) = T_0 \tag{34}$$

It a is well established tradition in fluid and thermal sciences to express the governing equations in ***dimensionless*** form. Nondimensionalization of equations helps to eliminate several physical constraints such as the use of particular units of measurements.

The dimensionless temperature U can be defined as

$$U = \frac{T - T_\infty}{T_0 - T_\infty} \tag{35}$$

and the dimensionless time τ as

$$\tau = \frac{\alpha t}{\ell^2} \tag{36}$$

where ℓ is some length scale to be judicially specified later.

Equations (31) and (32) can be, respectively, written in terms of the dimensionless temperature and time as

$$\frac{1}{(\sinh^2 \xi + \sin^2 \eta)}\left[\frac{1}{\sin\eta}\frac{\partial}{\partial \eta}(\sin\eta \frac{\partial U}{\partial \eta}) + \frac{1}{\sinh \xi}\frac{\partial}{\partial \xi}(\sinh \xi \frac{\partial U}{\partial \xi})\right] = \frac{c^2}{\ell^2}\frac{\partial U}{\partial \tau} \tag{37}$$

$$\frac{1}{(\sinh^2 \xi + \cos^2 \eta)}\left[\frac{1}{\sin\eta}\frac{\partial}{\partial \eta}(\sin\eta \frac{\partial U}{\partial \eta}) + \frac{1}{\cosh \xi}\frac{\partial}{\partial \xi}(\cosh \xi \frac{\partial U}{\partial \xi})\right] = \frac{c^2}{\ell^2}\frac{\partial U}{\partial \tau} \tag{38}$$

The boundary and initial conditions (33) and (34) can also be written in dimensionless form as

$$U(\eta,\xi_0,\tau)=0 \qquad U(\eta,0,\tau)<\infty \tag{39}$$

$$U(\eta,\xi,0)=1 \tag{40}$$

2.5 Methods of Solution

Two different solutions are presented for equation (37) subject to the boundary and initial conditions (39) and (40) with the understanding that a similar approach can be followed for equation (38). The first solution makes use of eigen function expansion with the spheroidal wave functions as basis, while the second is semi-numerical and makes use of a Legendre series expansion.

2.5.1 Solution in terms of spheroidal wave functions

Assuming that the solution of (37) admits the separation form

$$U = F(\eta,\xi)\Gamma(\tau) \tag{41}$$

It follows that

$$\frac{\left[\frac{1}{\sin\eta}\frac{\partial}{\partial\eta}(\sin\eta\frac{\partial F}{\partial\eta})+\frac{1}{\sinh\xi}\frac{\partial}{\partial\xi}(\sinh\xi\frac{\partial F}{\partial\xi})\right]}{(\sinh^2\xi+\sin^2\eta)F}=\frac{c^2}{\ell^2}\frac{\frac{d\Gamma}{d\tau}}{\Gamma}=-\lambda^2 \tag{42}$$

where $-\lambda^2$ is a separation constant which determines the type of heat movement.

By assuming further that $F(\eta,\xi)$ separates as $F=Z(\xi)\Phi(\eta)$, one finds that

$$\frac{\coth\xi\ Z' + Z''}{\left(\sinh^2\xi + \sin^2\eta\right)Z} + \frac{\cot\eta\ \Phi' + \Phi''}{\left(\sinh^2\xi + \sin^2\eta\right)\Phi} = \frac{c^2}{\ell^2}\frac{\Gamma'}{\Gamma} = -\lambda^2 \tag{43}$$

where the primes denote differentiation with respect to the appropriate variables.

Equation (43) may be separated again as

$$\frac{\cot\eta\ \Phi' + \Phi''}{\Phi} + \lambda^2\sin^2\eta = -\frac{\coth\xi\ Z' + Z''}{Z} - \lambda^2\sinh^2\xi = -\beta \tag{44}$$

where β is another separation constant.

Equation (44) with the transformations $\mu = \cos\eta$ and $\gamma = \cosh\xi$ can be written as

$$(1-\mu^2)\Phi'' - 2\mu\ \Phi' + \left[\lambda^2(1-\mu^2) + \beta\right]\Phi = 0\ ; -1 \le \mu = \cos(\eta) \le 1 \tag{45}$$

$$(1-\gamma^2)Z'' - 2\gamma\ Z' + \left[\lambda^2(1-\gamma^2) + \beta\right]Z = 0 \quad ; 1 \le \gamma = \cosh(\xi) \le \cosh(\xi_0) \tag{46}$$

The derivatives are now with respect to the variables μ and γ. Equations (45) and (46) are identical except for the range of μ and γ.

Spheroidal wave functions

The separated equations (45) and (46) are satisfied by the **Angular Wave Functions** $S_{mn}(\varepsilon,\mu)$ and the **Radial Wave Functions** $R_{mn}(\varepsilon,\gamma)$, respectively. These functions are also known as the spheroidal harmonics. This name originates from the fact that as the oblateness parameter $\varepsilon \to 0$, the angular functions $S_{mn}(\varepsilon,\mu) \to P_n^m(\mu)$, the associated Legendre functions, which apart from normalization and phase factors are essentially the popular spherical harmonics.

The eigenfunctions of equation (45), with the azimuthal wave number $m = 0$, are the angular wave functions of the first kind $S_{0n}^{(1)}(\lambda, \mu)$, and the angular wave functions of the second kind $S_{0n}^{(2)}(\lambda, \mu)$. On the other hand, the eigenfunctions of equation (46) are the radial wave functions of the first kind $R_{0n}^{(1)}(\lambda, \xi)$, and the radial wave functions of the second kind $R_{0n}^{(2)}(\lambda, \gamma)$. The eigenvalues $\beta = \beta(\lambda)$ are the same in the two equations (45) and (46). In the spherical limit $\lambda \to 0$, equation (45), with $\beta = n(n+1)$, is the Legendre equation. This similarity suggests that for $\lambda \neq 0$, one should consider an expansion in a series of associated Legendre functions. The angular wave functions of the first and second kinds are written, respectively, as

$$S_{mn}^{(1)}(\lambda, \mu) = \sum_{r=0,1}^{\infty}{}' d_r^{mn}(\lambda) P_{m+r}^{m}(\mu) \tag{47}$$

$$S_{mn}^{(2)}(\lambda, \mu) = \sum_{r=-\infty}^{\infty}{}' d_r^{mn}(\lambda) Q_{m+r}^{m}(\mu) \tag{48}$$

where P_{m+r}^{m} and Q_{m+r}^{m} are the associated Legendre functions of the first and second kinds, respectively, and d_r^{mn} are the coefficients of expansion. The prime on top of the summation indicates that the sum is performed over even values of r if $n-m$ is even and over odd values of r if $n-m$ is odd.

On the other hand, the radial wave functions of the first and second kinds are given by

$$R_{mn}^{(i)}(\lambda, \gamma) = \frac{(1-\gamma^{-2})^{m/2} \sum_{r=0,1}^{\infty}{}' (-1)^{\frac{r+m-n}{2}} d_r^{mn}(\lambda) \frac{(2m+r)!}{r!} \aleph_{m+r}^{(i)}(\lambda\gamma)}{\sum_{r=0,1}^{\infty}{}' d_r^{mn}(\lambda) \frac{(2m+r)!}{r!}} \tag{49}$$

where $\aleph_n^{(i)}$ is the i^{th} kind of Spherical Bessel Function of order n (i.e. $\aleph_n^{(1)}(\nu) = \sqrt{\frac{\pi}{2\nu}} J_{n+1/2}(\nu)$ and $\aleph_n^{(2)}(\nu) = \sqrt{\frac{\pi}{2\nu}} \Im_{n+1/2}(\nu)$ where J and $\Im$ are Bessel functions of the first and second kinds, respectively).

The computation of these spheroidal harmonics, however, is not trivial, and various methods have been studied by numerous authors such as the monographs by Flammer [7], and Stratton et al. [9]. Abramowitz and Stegun [8] compiled an excellent summary of the work on spheroidal functions, together with extensive tables of values. The solutions (spheroidal wave functions) are normalizable when $\beta_{mn}(\lambda)$ is a spheroidal eigenvalue. These eigenvalues are determined so that the wave functions are finite at ±1. Several normalizations are available. The popular Meixner- Schäfke scheme, [10], is chosen to work with. Unlike spherical systems, where they reduce simply to $n(n+1)$, the eigenvalues $\beta_{mn}(\lambda)$ are functions of λ. For details on calculations, in particular on the determination of the coefficients of the expansions in (47), (48) and (49), interested readers are referred to the excellent work of Faloon [6].

Figure 7 shows some typical graphs of the four spheroidal wave functions. The functions $S_{0n}^{(2)}(\lambda,\mu)$ and $R_{0n}^{(2)}(\lambda,\gamma)$ are not bounded on the domain of the problem under consideration. Therefore, The eigenfunctions of equations (45) and (46) reduce to only $S_{0n}^{(1)}(\lambda,\mu)$ and $R_{0n}^{(1)}(\lambda,\gamma)$. The full solution of equation (37) can now be written as

$$U(\eta,\xi,\tau) = \sum_{n=0}^{\infty}\sum_{k=1}^{\infty} A_{nk}\, S_{0n}^{(1)}(\lambda_{nk},\cos\eta)\, R_{0n}^{(1)}(\lambda_{nk},\cosh\xi)\, e^{\frac{-\ell^2}{c^2}\lambda_{nk}^2\,\tau} \tag{50}$$

where A_{nk} are the coefficients of the series, and the eigenvalues λ_{nk} are obtained from the boundary condition (39) as solutions of

$$R_{0n}^{(1)}(\lambda_{nk}, \cosh\xi_0) = 0, \quad n = 0,1,2,\ldots \quad , \quad k = 1,2,\ldots \tag{51}$$

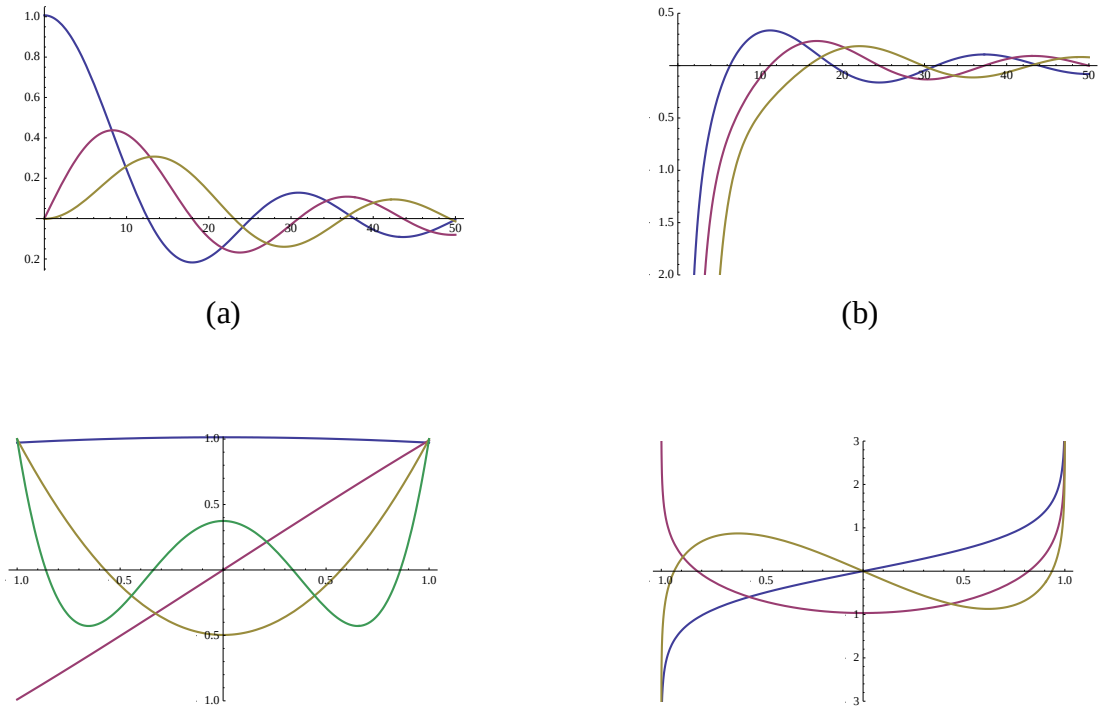

Figure 7: Typical graphs of spheroidal wave functions
(a) $R_{0n}^{(1)}$, **(b)** $R_{0n}^{(2)}$, **(c)** $S_{0n}^{(1)}$, **and (d)** $S_{0n}^{(2)}$

Table 1 lists the first few eigenvalues for the case of prolate spheroids with axis ratios $b/a = 0.5,\ 0.75,$ and 0.99. These values have been numerically computed using Mathematica 8.0 ®.

Table 1: Some values of $\lambda_{n\,k}$

b/a = 0.5	k = 1	2	3	4	5
n = 0	4.67462612151711	10.0357597681701	15.4552908480538	20.8865016479452	26.3220141660092
1	5.6810310487823	10.9832665193385	16.3877326812408	21.8120354262596	27.2435815524602
2	6.75090479817005	11.9650026232588	17.3431288636153	22.7548107966927	28.1789484697065
3	7.86836476049705	12.9776979135628	18.3201025304917	23.7140782312953	29.1276451484152
4	9.02109706334849	14.0183228082011	19.3173213392563	24.6891020795025	30.0892074831356
b/a = 0.75	k = 1	2	3	4	5
n = 0	2.55684004860736	5.26704432613836	8.02102176013003	10.7840803544045	13.5503717604929
1	3.39403517510938	6.06088208384699	8.79772524157625	11.5530623697167	14.3149122881915
2	4.26776181174174	6.89053216680837	9.59892678120084	12.3407182571788	15.0945622130174
3	5.15723050805737	7.75052944152041	10.4223570321317	13.1456500249859	15.8884008469122
4	6.04954937138634	8.63506426134211	11.2662033290643	13.9666269036966	16.6955824632366
b/a = 0.99	k = 1	2	3	4	5
n = 0	0.4461646824973	0.8924062855229	1.3387912714351	1.7853648868238	2.2321434143169
1	0.6364402049254	1.0942543427802	1.5446598797826	1.9928208584393	2.4400932038508
2	0.8168700404924	1.2889441785993	1.7462172441056	2.1982459996872	2.6477683086963
3	0.9905785161071	1.4766232161718	1.941579573031	2.3986064949819	2.8516408292299
4	1.1599886453140	1.6592863770838	2.1319508474031	2.5941915960897	3.0510619237689

To determine the coefficients A_{nk} in (50), an orthognality relation on the eigenfunctions is needed. Following Niven [5], if $U = F(\eta,\xi)\Gamma(\tau)$ is a solution of

$$\nabla^2 U = \frac{c^2}{\ell^2}\frac{\partial U}{\partial \tau} \tag{52}$$

then separation of variables results in

$$\nabla^2 F = -\lambda^2 F \tag{53}$$

Suppose that F_n and F_m are two solutions of (53) corresponding to the distinct eigenvalues λ_n and λ_m. Now, substitute F_n in (53) and then multiply by F_m and substitute F_m then multiply by F_n; subtracting the two resulting equations and integrating over the volume (υ) of the spheroid gives

$$(\lambda_n{}^2 - \lambda_m{}^2)\iiint_{\upsilon} F_n\, F_m\, d\upsilon = \iiint_{\upsilon} (F_n\,\nabla^2 F_m - F_m\,\nabla^2 F_n)\, d\upsilon \tag{54}$$

Using standard vector algebra, it is not difficult to show that, for ***distinct eigenvalues***, the right hand side of (54) is identically zero. The conclusion, then, is

$$\iiint_{\upsilon} F_n F_m \, d\upsilon = 0, \quad n \neq m \tag{55}$$

For a prolate spheroid, for example, using the two solutions $S_{0n}^{(1)}(\lambda_{nk}, \cos\eta) R_{0n}^{(1)}(\lambda_{nk}, \cosh\xi)$ and $S_{0m}^{(1)}(\lambda_{mj}, \cos\eta) R_{0m}^{(1)}(\lambda_{mj}, \cosh\xi)$ corresponding to the ***distinct eigenvalues*** λ_{nk} and λ_{mj}, and the fact that $d\upsilon = h_\phi h_\xi h_\eta \, d\phi d\xi d\eta$, one can rewrite (55), considering azimuthal symmetry, as

$$\int_{\eta=0}^{\pi} \int_{\xi=0}^{\xi_0} [S_{0n}^{(1)}(\lambda_{nk}, \cos\eta) R_{0n}^{(1)}(\lambda_{nk}, \cosh\xi) S_{0m}^{(1)}(\lambda_{mj}, \cos\eta) R_{0m}^{(1)}(\lambda_{mj}, \cosh\xi) \times (\sinh^2\xi + \sin^2\eta) \sinh\xi \sin\eta] \, d\xi d\eta = 0 \tag{56}$$

Applying the initial condition (40), the coefficients, A_{nk} in (50), can be determined using the relation

$$A_{nk} = \frac{\int_{\eta=0}^{\pi} \int_{\xi=0}^{\xi_0} S_{0n}^{(1)}(\lambda_{nk}, \cos\eta) R_{0n}^{(1)}(\lambda_{nk}, \cosh\xi) (\sinh^2\xi + \sin^2\eta) \sinh\xi \sin\eta \, d\xi d\eta}{\int_{\eta=0}^{\pi} \int_{\xi=0}^{\xi_0} [S_{0n}^{(1)}(\lambda_{nk}, \cos\eta) R_{0n}^{(1)}(\lambda_{nk}, \cosh\xi)]^2 (\sinh^2\xi + \sin^2\eta) \sinh\xi \sin\eta \, d\xi d\eta} \tag{57}$$

The solution (50) is, thus, complete.

2.5.2 Numerical solution using Legendre series expansion

The spheroidal wave functions are not as standard as, for example, Bessel functions or Legendre polynomials. These functions are programmed in the famous software

Mathematica®. Unfortunately, there are several problems associated with the current codes. The first obvious problem is the huge time it takes to generate the eigenvalues. The second, which is more serious, is that some of the spheroidal wave functions do not converge and start to oscillate for relatively large values of the arguments. One has to invoke several numerical procedure to obtain few eigenvalues and still uncertainty is always around. A numerical solution for the same considered problem has, therefore, been quite appealing.

Equation (37) can be written in terms of μ $(-1 \le \mu = \cos\eta \le 1)$ and γ $(1 \le \gamma = \cosh\xi \le \cosh\xi_0)$, as

$$\frac{1}{(\gamma^2-\mu^2)}\left[(\gamma^2-1)\frac{\partial^2 U}{\partial\gamma^2}+2\frac{\partial U}{\partial\gamma}+(1-\mu^2)\frac{\partial^2 U}{\partial\mu^2}-2\mu\frac{\partial U}{\partial\mu})\right]=\frac{c^2}{\ell^2}\frac{\partial U}{\partial\tau} \tag{58}$$

The dimensionless temperature is expanded in a series of the form

$$U(\gamma,\mu,\tau)=\sum_{n=0}^{\infty} f_n(\gamma,\tau)\,P_n(\mu) \tag{59}$$

where P_n is Legendre polynomial of the first kind. The choice of $P_n(\mu)$ comes from the fact that it is a solution in the angular direction for problems involving spherical geometries. Observe that this form, (59), satisfies the symmetry of the problem in the rotational direction.

Substituting the series (59) in equation (58) and using the orthogonality of Legendre functions, one, although a little tedious, can show that for $n \ge 0$

$$(\gamma^2-1)\frac{\partial^2 f_n}{\partial\gamma^2}+2\gamma\frac{\partial f_n}{\partial\gamma}-n(n+1)f_n=\frac{c^2}{\ell^2}\left[\gamma^2-\frac{2n^2+2n-1}{(2n-1)(2n+3)}\right]\frac{\partial f_n}{\partial\tau}$$
$$-\frac{c^2}{\ell^2}\frac{(n-1)n}{(2n-3)(2n-1)}\frac{\partial f_{n-2}}{\partial\tau}-\frac{c^2}{\ell^2}\frac{(n+2)(n+1)}{(2n+5)(2n+3)}\frac{\partial f_{n+2}}{\partial\tau} \tag{60}$$

where $n=0,1,2,\ldots$ and all functions with negative subscripts are identically zero. Note that the angular coordinate μ has been eliminated. The conditions (39) and (40) can be transferred onto the modes of the series (59). The second part of the boundary condition (39) $\left(\text{i.e. } U(\mu,\gamma=1,\tau)<\infty\right)$ is not useful for implementation in a numerical procedure. The needed second condition, along with $U(\mu,\cosh\xi_0,\tau)=0,$ is the vanishing slope of the temperature profile at $\xi=0$ (equivalently $\gamma=\cosh 0=1$). This condition can be written as

$$\frac{\partial U(\mu,1,\tau)}{\partial\gamma}=0 \tag{61}$$

Using the series (59), the boundary and initial conditions can be written on the modes of the series as

$$f_n(\gamma_0,\tau)=0 \tag{62}$$

$$\frac{\partial f_n(1,\tau)}{\partial\gamma}=0 \tag{63}$$

$$f_n(\gamma,0)=\delta_{n0} \tag{64}$$

where δ_{ij} is the Kronecker delta.

Assuming that the spheroid is introduced suddenly in the medium of constant temperature ($U=0$), the solution $U(\mu,\gamma,\tau)$ is advanced in time by solving (60) using a fully implicit

finite difference scheme. At time τ, the known solution at time $\tau - \Delta\tau$ is used as a starting solution to obtain the functions f_n sequentially (from $n = 0$ to $n_{\max}$, where $n_{\max}$ is the maximum number of terms used in the series (59)) using the most recently available information. The iterative procedure was tested against the step size (time and space) and the appropriate number of functions f_n needed. Following the sudden introduction of the spheroid into the medium, very small time steps were initially used.

Finite Difference method

The basic idea of this method is to approximate the differential equation by a system of algebraic equations. The system of algebraic equations is set up in a way such that the corresponding solution provides a good approximation for the solution of the differential equation.

The value of $f(x)$ at $a+h$ can be obtained from the Taylor series expansion

$$f(a+h) = f(a) + f'(a)h + \frac{f''(a)}{2!}h^2 + \ldots + \frac{f^{(n)}(a)}{n!}h^n + R_n(x) \tag{65}$$

where $R_n(x)$ is the remainder.

If $R_1(x)$ is sufficiently small, one can write

$$f'(a) \approx \frac{f(a+h) - f(a)}{h} \tag{66}$$

On the other hand, The value of $f(x)$ at $a-h$ can be obtained from the expansion

$$f(a-h) = f(a) - f'(a)h + \frac{f''(a)}{2!}h^2 - \ldots + (-1)^n \frac{f^{(n)}(a)}{n!}h^n + R_n(x) \tag{67}$$

Thus,

$$f'(a) \approx \frac{f(a) - f(a-h)}{h} \tag{68}$$

Adding (66) and (68) also gives

$$f'(a) \approx \frac{f(a+h) - f(a-h)}{2h} \tag{69}$$

The following difference formulas for $f''(a)$ can be obtained by manipulating (65) and (67).

$$f''(a) \approx \frac{f(a) - 2f(a+h) + f(a+2h)}{h^2} \tag{70}$$

$$f''(a) \approx \frac{f(a-2h) - 2f(a-h) + f(a)}{h^2} \tag{71}$$

$$f''(a) \approx \frac{f(a-h) - 2f(a) + f(a+h)}{h^2} \tag{72}$$

The formulas (66) and (70) are called **forward differences**, (68) and (71) are called **backward differences**, while (69) and (72) are the **central differences**. Forward differences and backward differences are needed for the boundary points since the points outside the boundary cannot be used.

Equations (60), using a fully implicit scheme with a time step size *k* and a spatial mesh size *h*, can be approximated by the algebraic equations

$$
\begin{aligned}
(\gamma_{i,j}^2-1)\left(\frac{f_n^{\,i+1,j}-2f_n^{\,i,j}+f_n^{\,i-1,j}}{h^2}\right)+2\gamma_{i,j}\left(\frac{f_n^{\,i+1,j}-f_n^{\,i-1,j}}{2h}\right)-n(n+1)f_n^{\,i,j} \\
=\frac{c^2}{\ell^2}\left[\gamma_{i,j}^2-\frac{2n^2+2n-1}{(2n-1)(2n+3)}\right]\left(\frac{f_n^{\,i,j}-f_n^{\,i,j-1}}{k}\right) \\
-\frac{c^2}{\ell^2}\frac{(n-1)n}{(2n-3)(2n-1)}\left(\frac{f_{n-2}^{\,i,j}-f_{n-2}^{\,i,j-1}}{k}\right) \\
-\frac{c^2}{\ell^2}\frac{(n+2)(n+1)}{(2n+5)(2n+3)}\left(\frac{f_{n+2}^{\,i,j}-f_{n+2}^{\,i,j-1}}{k}\right)
\end{aligned}
\tag{73}
$$

where $f^{\,i,j}$ represents the nodal value f $(\gamma = 1+ki, \tau = jk)$.

The implicit method requires an iterative procedure which is carried out by initializing $f_n; n = 0,1,2,...$ at the interior points for the new time step. The functions f_n are, then, updated using the most recently available information. The procedure is repeated until the values converge to the desired accuracy.

2.6 Discussion

2.6.1 Local Nusselt Number (N_u)

The local amount of heat transferred from the spheroid is

$$
q(\eta,t) = -K\left(\frac{1}{h_\xi}\frac{\partial T}{\partial \xi}\right)_{\xi=\xi_0} = -K\,(T_0-T_\infty)\left(\frac{1}{h_\xi}\frac{\partial U}{\partial \xi}\right)_{\xi=\xi_0} \tag{74}
$$

The **Nusselt number** is the rate of change of the heat across the boundary and normal to it. The local dimensionless Nusselt number is defined as

$$
N_u(\eta,\tau) = \frac{\ell\, q(\eta,\tau)}{K(T_0-T_\infty)} = -\ell\left(\frac{1}{h_\xi}\frac{\partial U}{\partial \xi}\right)_{\xi=\xi_0} \tag{75}
$$

2.6.2 Average Nusselt number ($\overline{N_u}$)

The average Nusselt number is calculated by averaging the local Nusselt number over the surface. So, at a given τ,

$$\overline{N_u}(\tau) = \frac{\int_S N_u(\eta,\tau)\,ds}{\Omega} = \frac{\int_{\varphi=0}^{2\pi}\int_{\eta=0}^{\pi} N_u(\eta,\tau)\,h_\eta h_\varphi\,d\eta\,d\varphi}{\Omega} \tag{76}$$

where $\Omega = \int_{\varphi=0}^{2\pi}\int_{\eta=0}^{\pi} h_\eta h_\varphi\; d\eta\; d\varphi$ is the surface area of the spheroid and is given, for a prolate spheroid, by

$$\Omega_{\text{prolate}} = 2\pi b^2\left[1+\frac{1}{(b/a)\sqrt{1-(b/a)^2}}\sin^{-1}\sqrt{1-(b/a)^2}\right] \tag{77}$$

and for an oblate spheroid by

$$\Omega_{\text{oblate}} = 2\pi a^2\left[1+\frac{(b/a)^2}{\sqrt{1-(b/a)^2}}\tanh^{-1}\sqrt{1-(b/a)^2}\right] \tag{78}$$

2.6.3 Average nondimensional Temperature, $\overline{U}(\tau)$

It is of interest to calculate the average temperature inside the spheroid as time progresses. That serves as a measure of the amount of energy that has remained in the spheroid (or equivalently, has been transferred to the surrounding medium). Averaging the dimensionless temperature inside the spheroid is carried according to the formula

$$\overline{U}(\tau) = \frac{\int U(\eta,\xi,\tau)\,d\upsilon}{\upsilon} \tag{79}$$

The volume of the spheroid, υ, is given for a prolate spheroid by

$$\upsilon_{\text{prolate}} = \frac{4}{3}\pi a b^2 \tag{80}$$

and for an oblate spheroid by

$$\upsilon_{\text{oblate}} = \frac{4}{3}\pi a^2 b \tag{81}$$

Limiting Case of Sphere

The limiting case for a spheroid as $\xi \to \infty$ is a sphere. Consider a sphere of radius a_s initially heated to a uniform temperature T_0 and then left to cool in an infinite medium of constant temperature T_∞. Taking into account the angular and azimuthal symmetries, the heat equation (30) in spherical coordinates (r, θ, ϕ) reduces to

$$\frac{\partial^2 T}{\partial r^2} + \frac{2}{r}\frac{\partial T}{\partial r} = \frac{1}{\alpha}\frac{\partial T}{\partial t} \tag{82}$$

Once again, define the dimensionless temperature $U = \frac{T - T_\infty}{T_0 - T_\infty}$, the dimensionless time $\tau = \frac{\alpha t}{a_s^2}$, and the dimensionless radial distance $\rho = \frac{r}{a_s}$. The energy equation (82) can be written as

$$\frac{\partial^2 U}{\partial \rho^2} + \frac{2}{\rho}\frac{\partial U}{\partial \rho} = \frac{\partial U}{\partial \tau} \tag{83}$$

It is a simple exercise to show that the solution of the last equation, independent of θ, is

$$U(\rho, \tau) = \sum_{i=1}^{\infty} \frac{2(-1)^{i+1} \sin(i\pi\rho)}{i\pi\rho} e^{-i^2\pi^2\tau} \tag{84}$$

Averaging the dimensionless temperature inside the sphere gives the simple formula

$$\bar{U}(\tau) = \frac{\int_{\upsilon} U(\rho,\tau)\, d\upsilon}{\upsilon} = \frac{6}{\pi^2}\sum_{i=1}^{\infty}\frac{e^{-i^2\pi^2\tau}}{i^2} \tag{85}$$

Nusselt number, in this case, varies only with τ due to the angular and azimuthal symmetries. It is defined through scaling the heat flow rate by $(T_0 - T_\infty)$, K, and the radius of the sphere a_s and can be calculated as

$$N_u(\tau) = \frac{a_s\, q(\tau)}{K\,(T_0 - T_\infty)} = -\left(\frac{\partial U}{\partial \rho}\right)_{\rho=1} = 2\sum_{i=1}^{\infty} e^{-i^2\pi^2\tau} = -1 + \vartheta_3(0, e^{-\pi^2\tau}) \tag{86}$$

where ϑ_3 is a Jacobi Elliptic Theta Function. The average Nusselt number, $\overline{N_u}(\tau)$, in the sphere case is identical to $N_u(\tau)$ due to the angular symmetry.

2.7 Results

The temperature inside a spheroid is affected by the axis ratio b/a and the elapsed time, τ. Considering the length scale, ℓ, to be the semi-major axis of the spheroid (i.e. $\ell = a$) facilitates comparing spheroids having the same length of the major axis and different axis ratios.

Figure 8(a) shows a comparison of Nusselt numbers between the solution in spheroidal wave functions (the dotted lines), and the semi-numerical solution (the solid lines) at $\tau = 0.1$. The Nusselt number of the limiting case of sphere is also shown. **Figure 8(b)** and **Figure 8(c)**, respectively, show the variation of the average Nusselt number on the

surface and average temperature with time for the same cases. A good agreement is observed between the two solutions.

The solutions in terms of spheroidal wave functions are obtained using only six eigenfunctions with six eigenvalues each. On the other hand, in the implicit finite difference scheme, several choices of the space and time discritization schemes were tested. Eventually, the number of terms taken in the series was $n_{\max} = 30$. Three hundred points were considered in the radial direction, and a dynamic time step scheme was used. At the start of simulation, very small time steps were used as the temperature gradient was very high. Smaller time steps were subsequently used. A tolerance of 10^{-8} between consecutive iterations in the iteratively computed values of the temperature was set.

Figure 9 shows the time development of the isotherms inside a prolate spheroid of $b/a = 1/2$. The initially high heat transfer rate on the surface which has little influence on the temperature deeper inside the spheroid subsides with time.

The time development of the heat transfer rate on the surface of a prolate spheroid of $b/a = 1/2$ is shown in **Figure 10(a)** while that for an oblate spheroid of $b/a = 1/2$ is shown in **Figure 10(b)**. The maximum heat transfer rate, in the case of a prolate spheroid, occurs at $\eta = 90^o$ (i.e. at the flat part or minimum curvature), while it occurs at $\eta = 0^o, 180^o$ (again at the flat portions) in the case of an oblate spheroid.

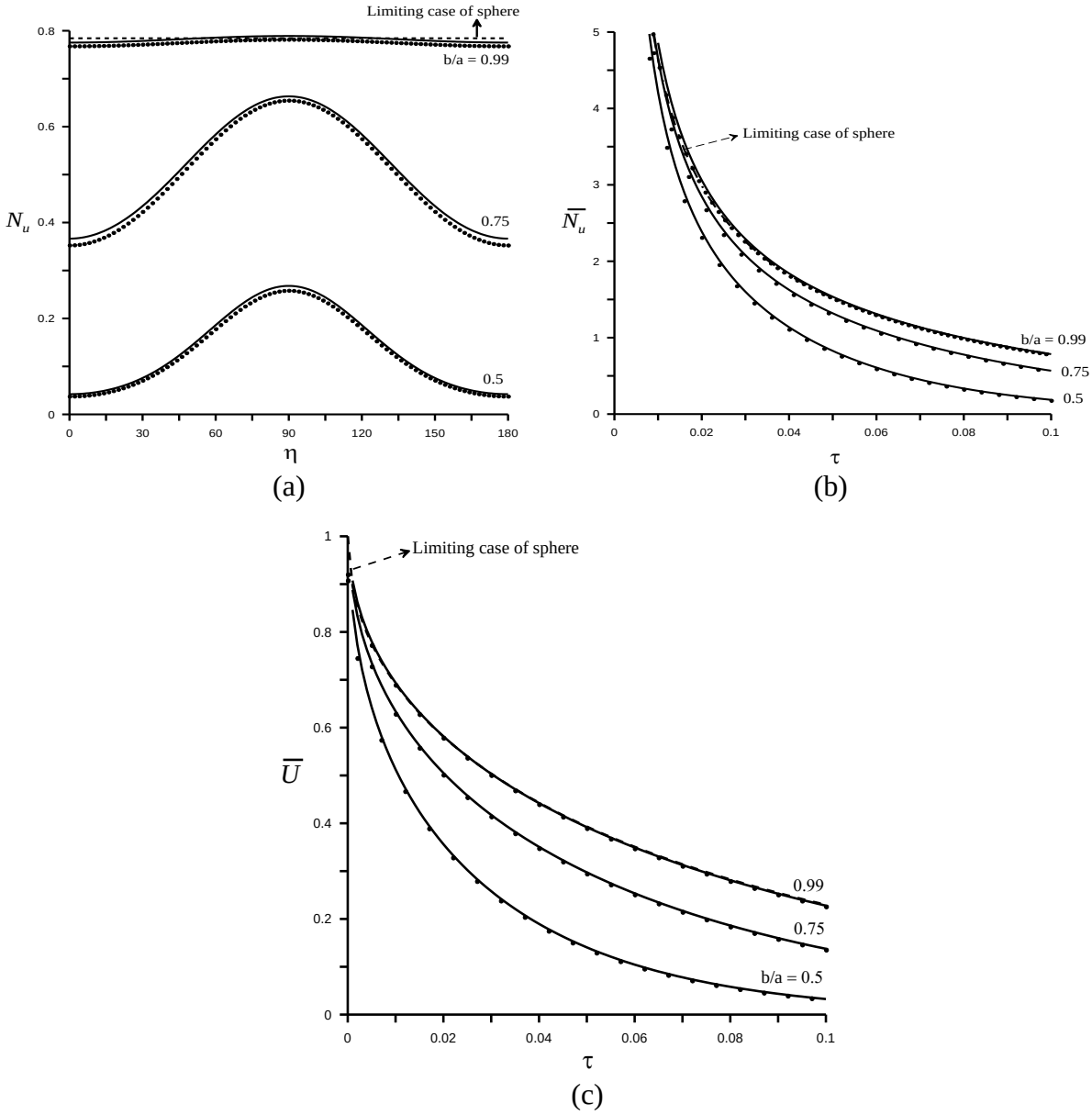

Figure 8: (a) N_u **at** $\tau = 0.1$**, (b)** $\overline{N_u}$ **, (c)** $\overline{U}$
for prolate spheroids using spheroidal wave functions (dotted lines), and using the numerical solution (solid lines).

Figure 11 shows isotherms for oblate spheroids with varying axis ratios at $\tau = 0.01$.

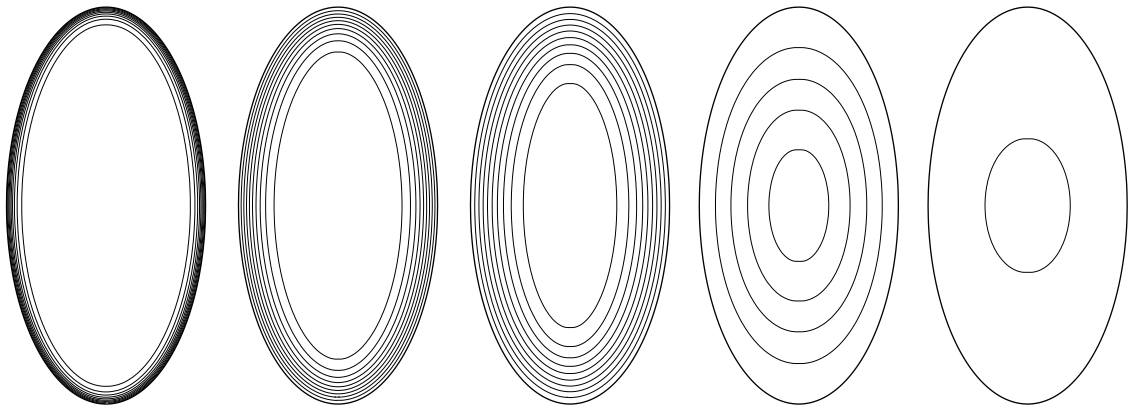

Figure 9: Time development of the isotherms inside a prolate spheroid of $b/a = 1/2$. (a) $\tau = 0.001$, (b) $\tau = 0.005$, (c) $\tau = 0.01$, (d) $\tau = 0.05$, (e) $\tau = 0.1$

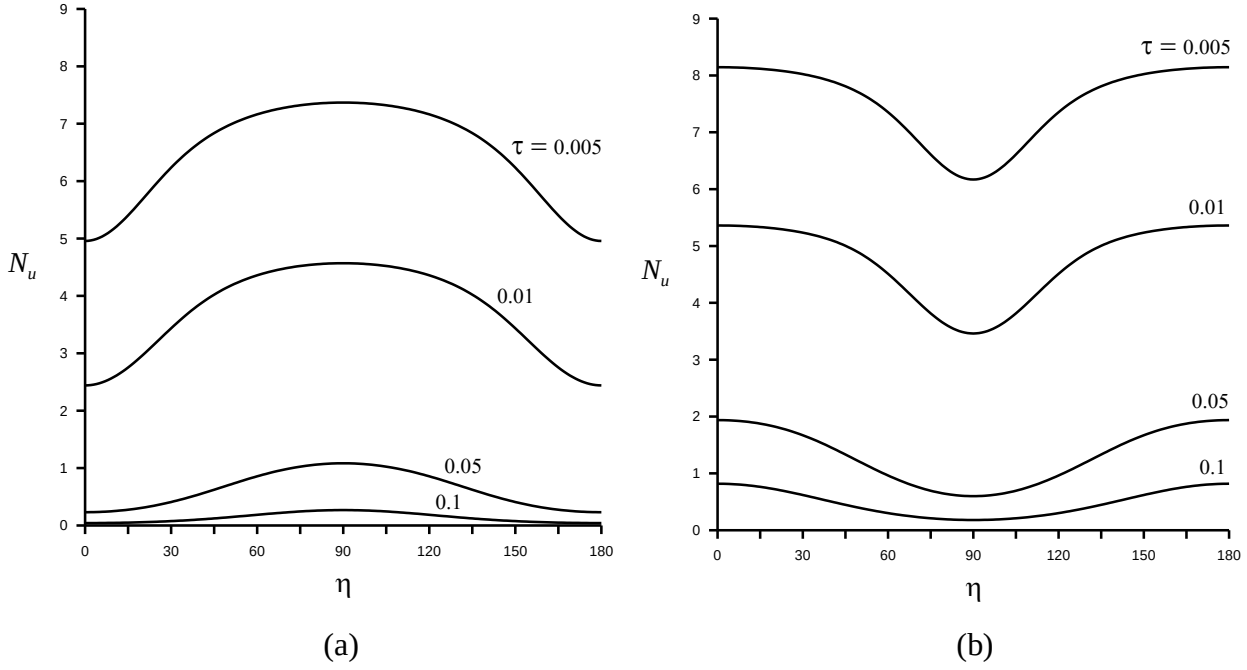

Figure 10: Time development of N_u on the surface of the spheroid of $b/a = 1/2$. (a) Prolate, (b) Oblate

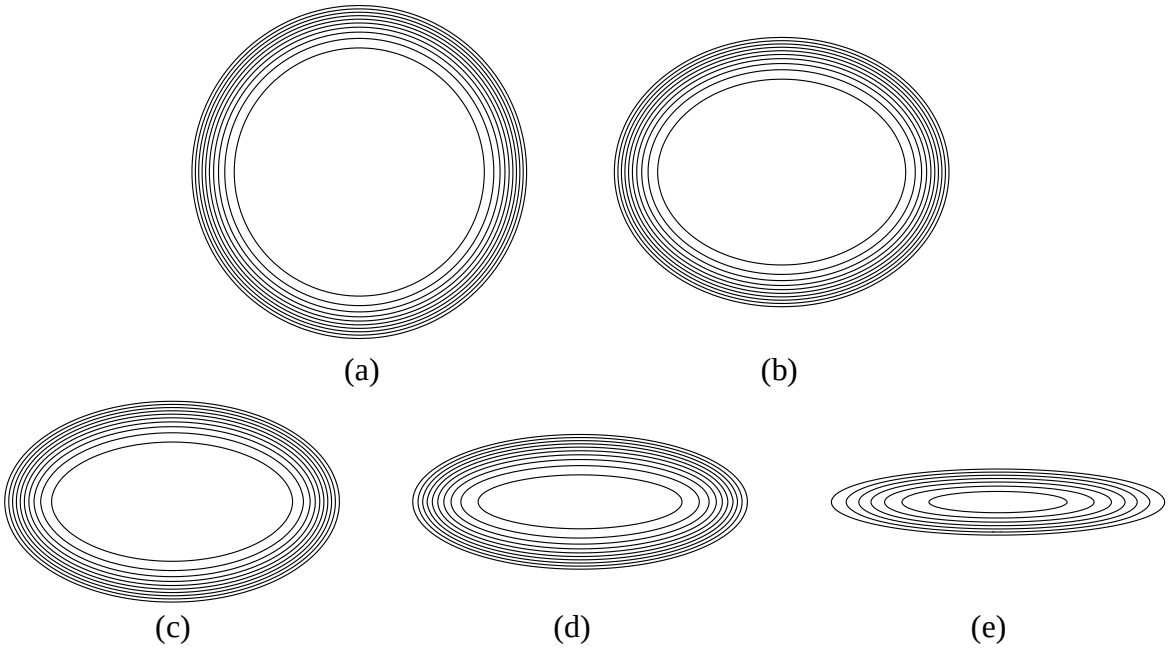

Figure 11: Isotherms in increments of 0.01 inside oblate spheroids of varying axis ratios.

(a) $b/a = 0.99$**, (b)** $b/a = 0.8$**, (c)** $b/a = 0.6$**, (d)** $b/a = 0.4$**, (e)** $b/a = 0.2$

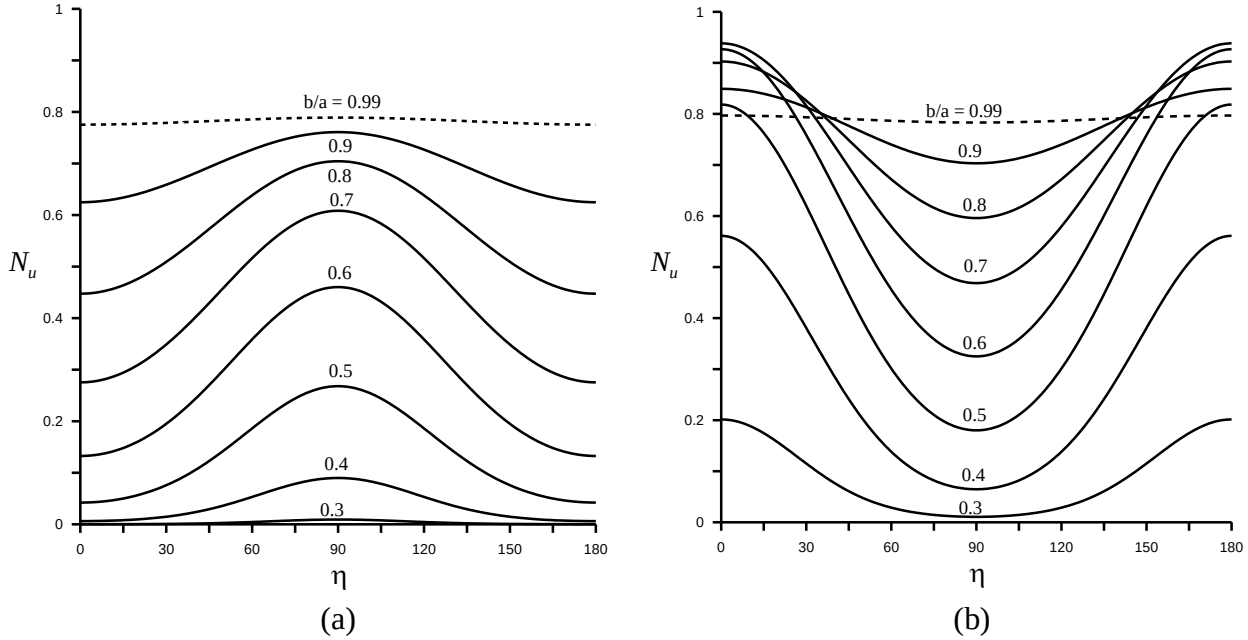

Figure 12: N_u **on the surface of spheroids of varying axis ratios at** $\tau = 0.1$**.**

(a) Prolate, (b) Oblate

Figure 12 shows Nusselt number distribution on the surface for spheroids with varying axis ratios at $\tau = 0.1$. The temperature variations from the surface of a spheroid to its core may suggest to calculate the average temperature, $\overline{U}(\tau)$ in equation (79), as a measure of the energy remaining inside the spheroid. **Figure 13** shows the development of $\overline{U}(\tau)$ for prolate and oblate spheroids with different axis ratios. The figure indicates that prolate spheroids lose energy faster than oblate spheroids for the same axis ratios. One should not forget, however, that prolate spheroids are smaller in volume than oblate spheroids with equal major axes and equal axis ratios

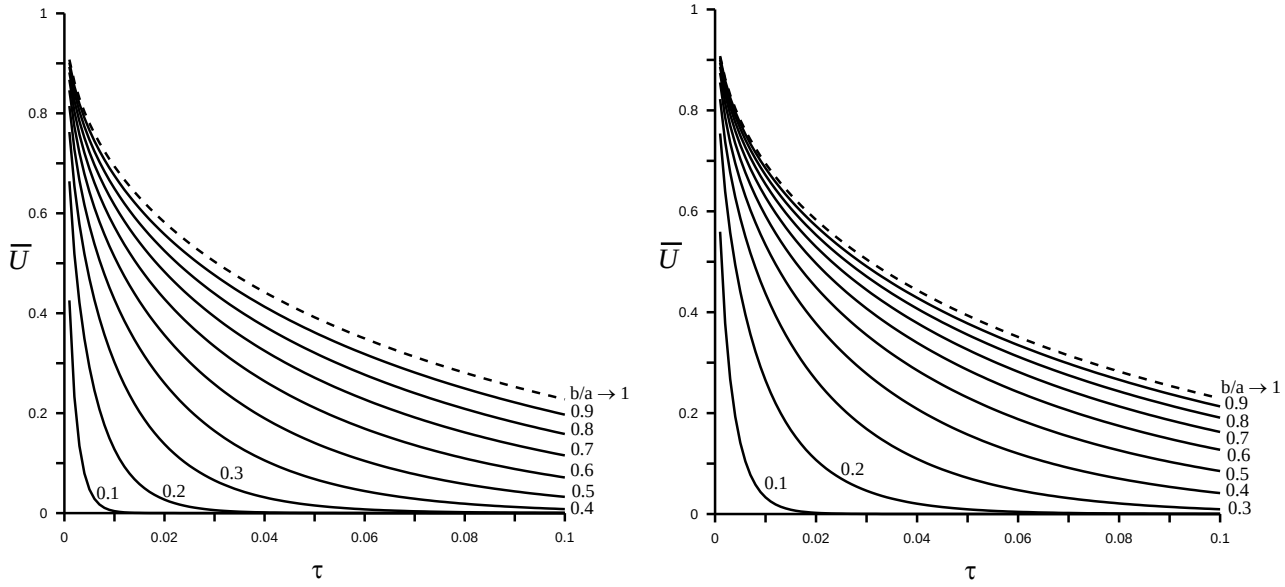

Figure 13: Development of $\overline{U}$ for spheroids of varying axis ratios. (a) Prolate, (b) Oblate

So far, the comparisons between spheroids are based on the length scale, ℓ, taken as the semi-major axis of the spheroid (i.e. $\ell = a$). This practically means that all the spheroids

have the same length of the major axis. Obviously, comparing two spheroids with equal major axes may not be "fair" as their two volumes are obviously different. It would be reasonable to compare spheroids having different axis ratios but the same volume. Therefore, one should consider those spheroids with volumes equal to the volume of a unit sphere ($a_s = 1$). In such cases, the spheroids may have different major axes in addition to different minor axes. The major and minor axes of a spheroid are consequently related by $ab^2 = 1$ in the case of a prolate spheroid, and by $a^2 b = 1$ for an oblate spheroid. An obvious length scale to be used for such cases is the radius of the unit sphere a_s. **Figure 14** displays isotherms for prolate spheroids with varying axis ratios and constant volume at $\tau = 0.05$.

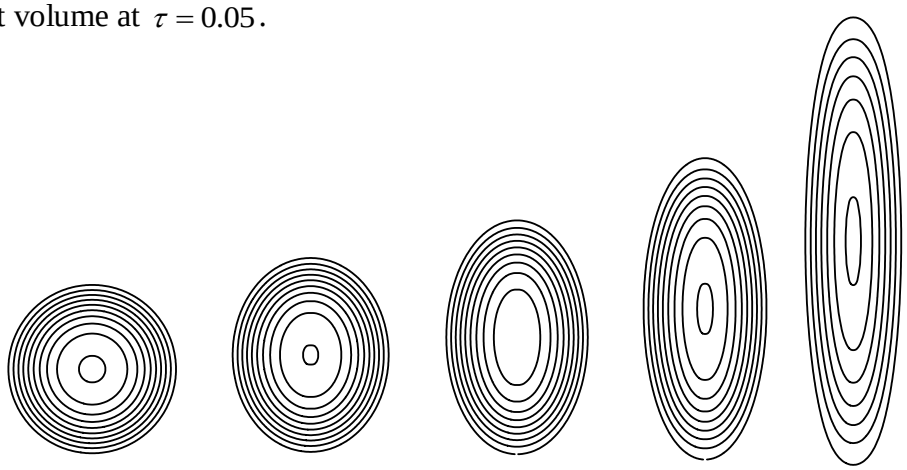

Figure 14: Isotherms in increments of 0.05 inside prolate spheroids of constant volumes.
(a) $b/a = 0.99$, **(b)** $b/a = 0.8$, **(c)** $b/a = 0.6$, **(d)** $b/a = 0.4$, **(e)** $b/a = 0.2$

Figure 15 presents local Nusselt numbers for spheroids with different axis ratio and constant volumes at $\tau = 0.01$ while **Figure 16** shows the average values up to $\tau = 0.01$ of **Figure 15**.

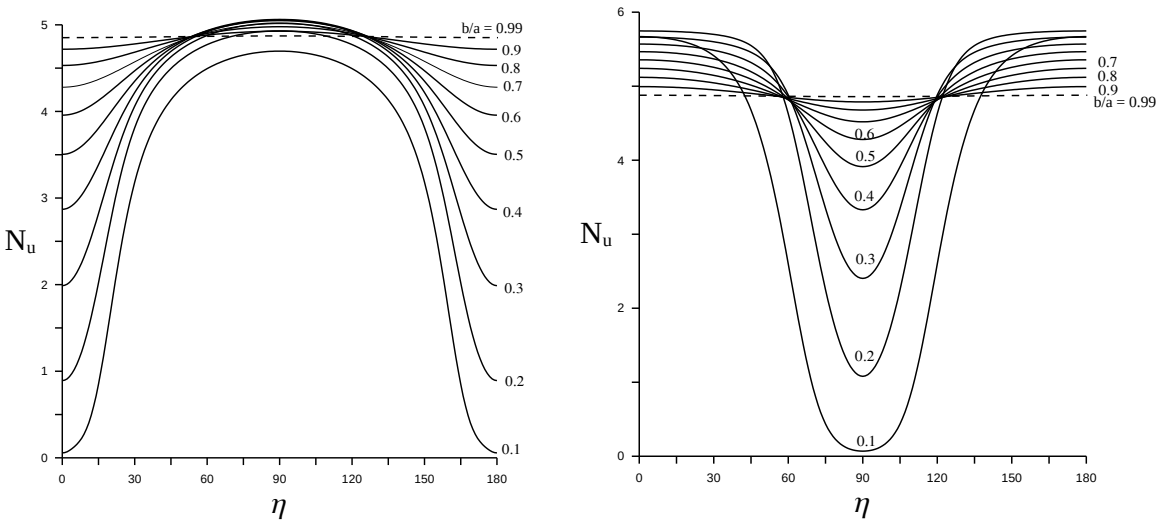

Figure 15: Local Nusselt numbers for different axis ratios and constant volumes at $\tau = 0.01$.
(a) Prolate, (b) Oblate

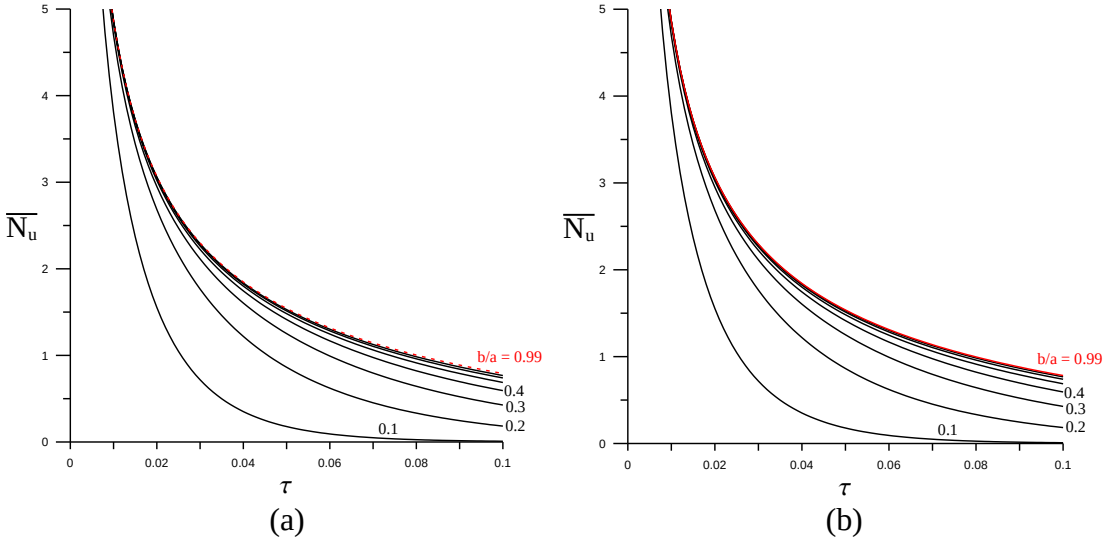

Figure 16: Average Nusselt number for spheroids of equal volume.
(a) Prolate, (b) Oblate

Figure 17 shows the development of $\overline{U}(\tau)$ for prolate and oblate spheroids with equal volumes. An interesting feature of the figures is that for small axis ratios, an oblate spheroid transfers heat to the infinite medium faster than a prolate spheroid with the same

axis ratio and the same volume. For large axis ratios, there is little dependence of the heat transfer rate on the axis ratio. Furthermore, there is no significant difference in the heat transfer rate for spheroids of either type. This is not unexpected and can be well explained by the fact that, for small axis ratios, the surface area of an oblate spheroid is much larger than the surface area of a prolate spheroid which has the same volume. At large axis ratios, as shown in **Figure 18**, the two surface areas are almost equal.

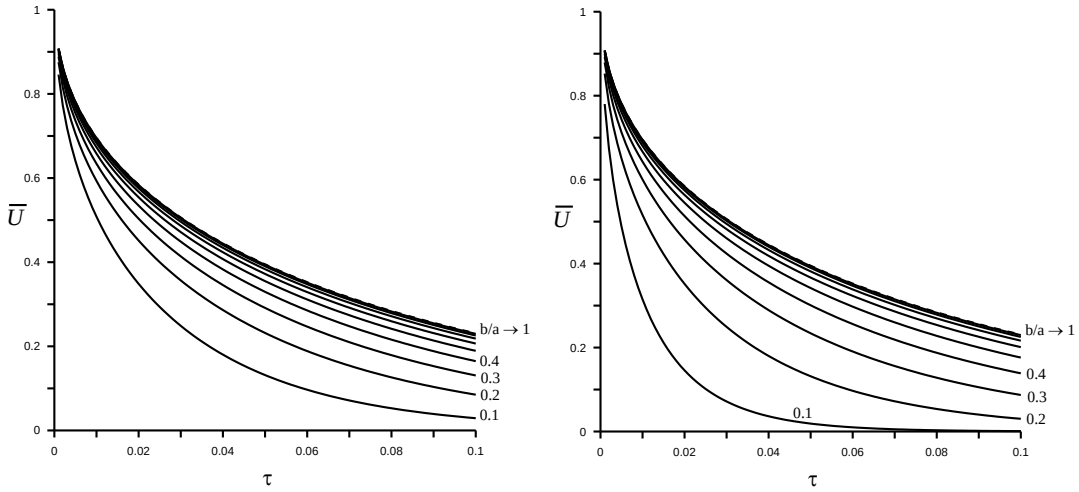

Figure 17: Development of $\overline{U}$ for spheroids of equal volume.
(a) Prolate, (b) Oblate

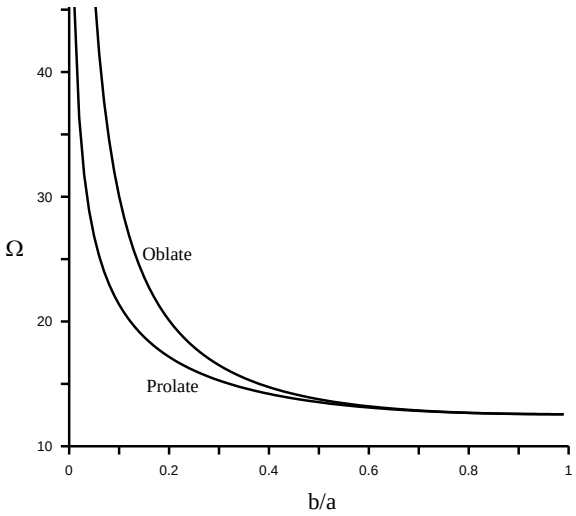

Figure 18: Surface area of spheroids with volumes equal to unit sphere

CHAPTER 3: Hagen-Poiseuille Flow in a Semi-Elliptic Tube

3.1 Introduction

Microchannels are fine tubes, approximately the width of a human hair, etched into a silicon wafer. These channels offer high surface area per volume ratios, high heat transfer coefficients, and low thermal resistances, Bahrami [18]. In addition to connecting different devices, microchannels are also utilized as biochemical reaction chambers, in physical particle separation, in inkjet print heads, in infrared detectors, in diode lasers, for cooling computer chips, and numerous other applications. An interesting application of this technology is the Microchannel Flow Analyzer which is basically a blood flow analysis instrument gaining popularity among health conscious people, Minamitani [19]. This instrument can visualize blood flow in narrow channels whose size is similar to human capillaries. Depending on the physical condition of the patients, the blood flow can reveal problems such as red blood cells' ability to deform. Due to these numerous applications, fluid flow in microchannels has emerged as an important research area.

Industrial techniques used to manufacture microfluidic devices produce microchannels of several cross-sections. In addition to the classical circular cross-sections, microfabrication also produces channels with non-circular cross-sections such as rectangular, elliptic, and trapezoidal which have wide practical applications in Micro-Electro-Mechanical Systems (MEMS), [20, 21]. The third most common microchannel geometry could be the semi-circular profile, which occurs naturally in hard micromachining with isotropic etching, [22, 23, 24]. The semicircular microchannels that

are fabricated using hard or soft micromachining have, in fact, semi-elliptic cross-sections instead, where the axis ratio of such sections is not unity.

Understanding the characteristics of flow through microchannels is very important in determining pressure distribution, heat transfer, and transport properties of the flow. Exact analytical solutions for the flow in channels with no-slip boundary conditions have been obtained in the literature only for very simple geometry of channel sections such as circular and rectangular sections. No exact solution of the flow problem within a straight microchannel of semi-elliptic cross-section is known.

3.2 Problem Statement

Consider the flow thorough a straight microchannel having a semi-elliptic cross-sectional area. The corresponding full ellipse has major and minor axes of length 2*a* and 2*b* respectively, with $c = \sqrt{a^2 - b^2}$ being the focal distance, **Figure 19**. The present model is based on assuming a fully developed steady laminar flow, constant fluid properties, negligible slip on the walls and surface effects, and negligible body forces. For such a flow, the Navier-Stokes equations reduce to the two dimensional momentum (Poisson's) equation

$$\nabla^2 w = \frac{1}{\mu}\frac{dP}{dz} \tag{87}$$

where w is the fluid velocity, P is the pressure, μ is the dynamic viscosity of the fluid, and z is the direction of the flow. The boundary condition, to be considered, is that the

velocity is zero on the wall of the channel, that is $w = 0$ everywhere on the wall of the channel.

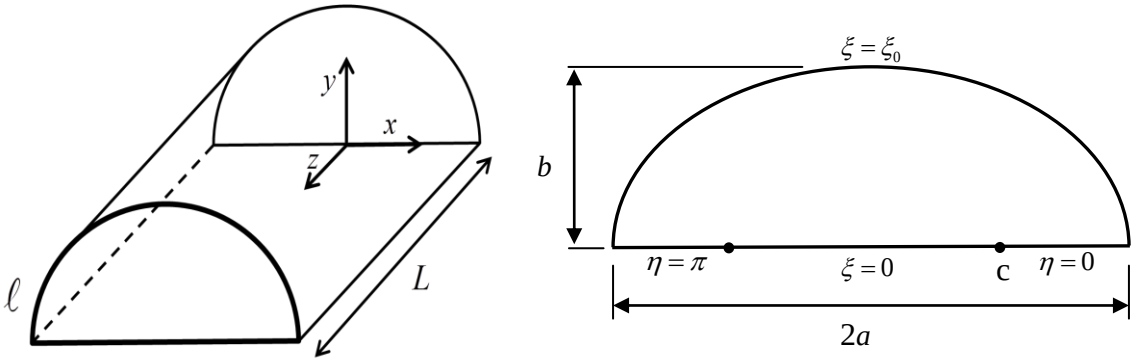

(a) **(b)**

Figure 19: Problem configuration
(a) A segment of length *L* from the channel, (b) Cross section of the channel perpendicular to the direction of the flow

3.3 Elliptic Cylindrical Coordinates System

The elliptic cylindrical coordinates (η, ξ, z) is the proper coordinates system that coincides with the boundary surface of the region. This coordinates system is generated by extending an ellipse along the *z*-axis. It is related to the Cartesian coordinates system by

$$\begin{aligned} x &= c\ \cosh\xi\cos\eta \\ y &= c\ \sinh\xi\sin\eta \\ z &= z \end{aligned} \tag{88}$$

where $(0 \le \xi < \infty)$, $(0 \le \eta < 2\pi)$, and $(-\infty < z < \infty)$.

The elliptic cylindrical coordinates, **Figure 20**, has the following coordinate surfaces:

- Elliptic cylinders, (ξ = constant), $\dfrac{x^2}{c^2\cosh^2\xi} + \dfrac{y^2}{c^2\sinh^2\xi} = 1$

- Hyperbolic cylinders, (η = constant), $\dfrac{x^2}{c^2\cos^2\eta} - \dfrac{y^2}{c^2\sin^2\eta} = 1$

- Planes parallel to *xy*-plane, (*z* = constant)

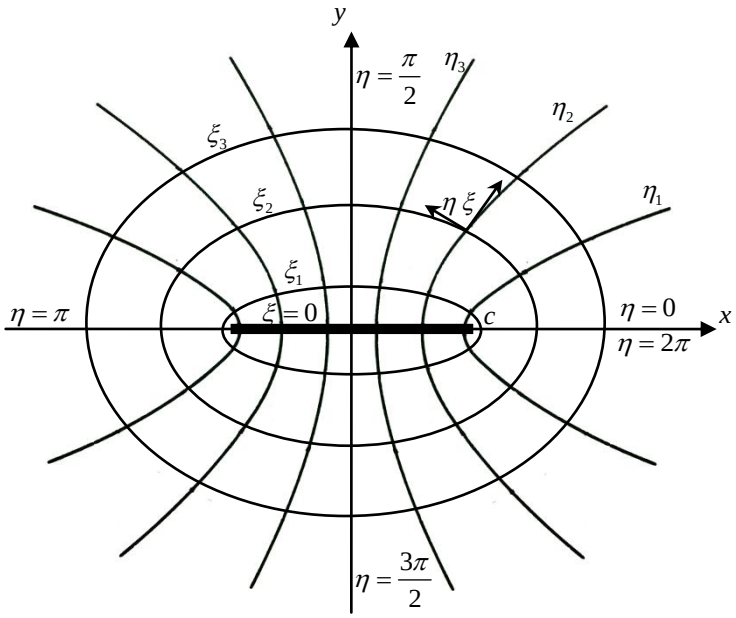

Figure 20: Elliptic cylindrical coordinates

The corresponding scale factors are

$$h_\xi = h_\eta = c\sqrt{\sinh^2\xi + \sin^2\eta}, \qquad h_z = 1 \tag{89}$$

An infinitesimal element of area on the cross-section, and an infinitesimal volume element are given by

$$dA = h_\xi h_\eta d\xi d\eta = 1 = c^2\left(\sinh^2\xi + \sin^2\eta\right) d\xi d\eta \tag{90}$$

$$dV = h_\xi h_\eta h_z d\xi d\eta dz = c^2\left(\sinh^2\xi + \sin^2\eta\right) d\xi d\eta dz \tag{91}$$

The surface of the channel is obtained when $\xi = \xi_0$ which is related to the axis ratio *b/a* by $\xi_0 = \tanh^{-1}(b/a)$. Hence, the values of the coordinates variables on the four segments of the wall are as shown in **Figure 19(b)**.

3.4 Governing Differential Equation and Boundary Conditions

Since the velocity profile is fully developed along the *z*-coordinate (i.e. $\frac{\partial w}{\partial z} = 0$), equation (87) can be expressed in elliptic cylindrical coordinates as

$$\frac{1}{c^2\left(\sinh^2\xi + \sin^2\eta\right)}\left[\frac{\partial^2 w}{\partial \xi^2} + \frac{\partial^2 w}{\partial \eta^2}\right] = \frac{1}{\mu}\frac{dP}{dz} \tag{92}$$

The dimensionless velocity, $u(\xi,\eta)$, is defined as

$$u = w \,/\, (-\frac{a^2}{\mu}\frac{dP}{dz}) \tag{93}$$

Equation (92) can be written in terms of the dimensionless velocity as

$$\frac{1}{\sinh^2\xi + \sin^2\eta}\left(\frac{\partial^2 u}{\partial \xi^2} + \frac{\partial^2 u}{\partial \eta^2}\right) = -\operatorname{sech}^2\xi_0 \tag{94}$$

The boundary conditions can also written as

$$u(\xi,0) = u(\xi,\pi) = u(0,\eta) = u(\xi_0,\eta) = 0 \tag{95}$$

3.5 Infinite Series Expansion Solution

One can observe that a particular solution of the non-homogeneous partial differential equation (94) is $-\frac{1}{2}\sinh^2\xi\,\sin^2\eta\,\mathrm{sech}^2\,\xi_0$. The general solution may, then, be written as

$$u = -\frac{1}{2}\sinh^2\xi\,\sin^2\eta\,\mathrm{sech}^2\,\xi_0 + \sum_{n=1}^{\infty} c_n \sin(n\eta)\sinh(n\xi) \tag{96}$$

The boundary condition at $\xi = \xi_0$ along with the orthognality of the eigenfunctions gives the required expression for c_n as

$$c_n = \frac{2\tanh^2\xi_0}{\pi\sinh(n\xi_0)}\frac{\left[\cos(n\pi)-1\right]}{n(n-2)(n+2)} \quad ; n = 1,2,3,.. \tag{97}$$

The full solution of (94) and (95), now, is

$$u = -\frac{1}{2}\mathrm{sech}^2\xi_0\sinh^2\xi\sin^2\eta - \frac{4}{\pi}\tanh^2\xi_0\sum_{n=1}^{\infty}\frac{\sin(2n-1)\eta\,\sinh(2n-1)\xi}{(2n-1)(2n-3)(2n+1)\sinh(2n-1)\xi_0} \tag{98}$$

3.6 Discussion

3.6.1 Nondimensional velocity distribution

Figure 21 shows the dimensionless velocity distribution in a channel with $b/a = 1/2$.

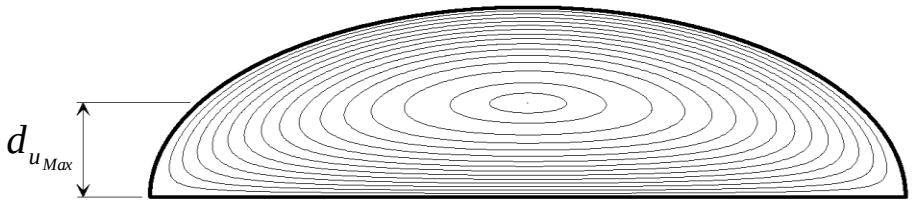

Figure 21: Velocity distribution for the case $b/a = 1/2$

3.6.2 Maximum nondimensional velocity

Due to the symmetry of the channel, the maximum nondimensional velocity is at $\eta = \pi/2$. The distance $d_{u_{Max}}$, at which the maximum velocity occurs, **Figure 21**, can be found by setting $\left.\frac{\partial u}{\partial \xi}\right|_{\eta=\pi/2} = 0.$

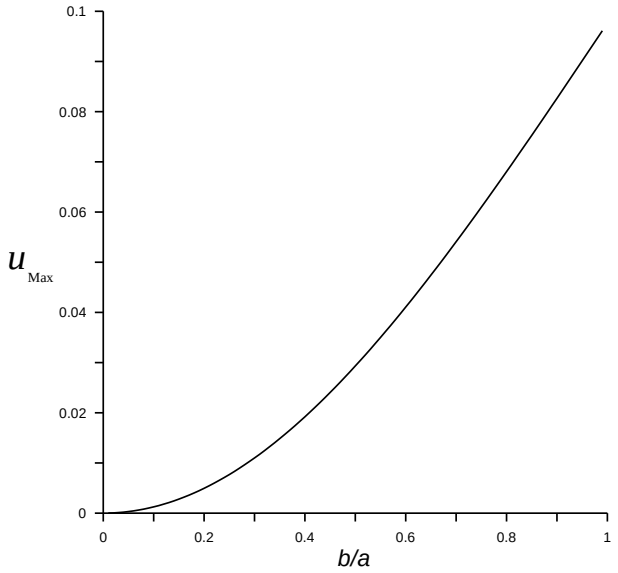

Figure 22: Maximum dimensionless velocity

The magnitude of the maximum velocity depends on the axis ratio b/a, as shown in **Figure 22**. The maximum dimensionless velocity increases to its largest value when the channel is semi-circular, i.e. $b/a = 1$.

3.6.3 Average dimensionless velocity

The average dimensionless velocity, $\bar{u}$, in the channel is calculated by

$$\bar{u} = \frac{\int_A u\, dA}{A} \tag{99}$$

where $A = \pi ab/2$ is the area of the cross-section of the semi-elliptic channel. Using the expression for u given in (98), the average velocity can be written as

$$\bar{u} = \frac{1}{4}\tanh^2 \xi_0 - \frac{16}{\pi^2}\tanh^3 \xi_0 \sum_{n=1}^{\infty} \frac{\coth(2n-1)\xi_0}{(2n-1)(2n+1)^2(2n-3)^2} \tag{100}$$

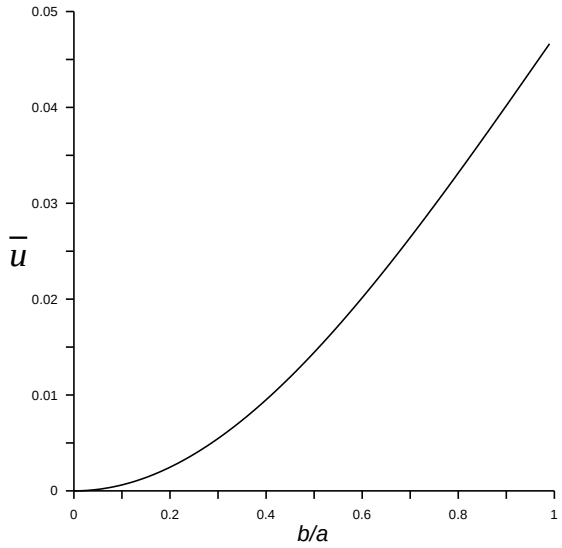

Figure 23: Average nondimensional velocity

The average dimensionless velocity also increases to its largest value as the axis ratio approaches unity, **Figure 23**. The average dimensionless velocity for the limiting case as $b/a \to 1$ (or $\xi_0 \to \infty$) is $\bar{u} \to \frac{1}{4} - \frac{2}{\pi^2}$. This limiting value is identically that obtained from carrying the same analysis in polar coordinates (r, θ, z) for a semicircular cross-section of radius a. Omitting the details, one can write the solution of the dimensionless velocity for the flow in a semicircular section as

$$u(R,\theta) = -\frac{R^2 \sin^2\theta}{2} - \frac{4}{\pi}\sum_{k=1}^{\infty} \frac{R^{2k-1}\sin(2k-1)\theta}{(2k-3)(2k-1)(2k+1)} \tag{101}$$

where $R = r/a$. Averaging the dimensionless velocity, the limiting value $\frac{1}{4} - \frac{2}{\pi^2}$ is obtained.

3.6.4 Shear stress

Shear stress, denoted by σ, is defined as the component of stress coplanar with a material cross-section. It arises from the force vector component parallel to the cross-section.

The dimensionless shear stress, τ, is defined as

$$\tau = -\frac{\sigma}{a\frac{dP}{dz}} \tag{102}$$

The shear stress acting on any of the four segments comprising the semi-elliptic channel shown in **Figure 19(b)** is either $\sigma_{\xi z}$ (on $\xi = \xi_0$ and $\xi = 0$) or $\sigma_{\eta z}$ (on $\eta = 0$ and $\eta = \pi$). These stresses are related to the velocity gradients by the relations

$$\tau_{\xi,z} = \frac{a}{h_\xi}\frac{\partial u}{\partial \xi} \tag{103}$$

$$\tau_{\eta,z} = \frac{a}{h_\eta}\frac{\partial u}{\partial \eta} \tag{104}$$

Using equations (98), (103), and (104) and taking the appropriate signs, the following expressions for the dimensionless shear stress on the four segments of the channel are obtained

$$\tau_{\xi,z}\Big|_{\xi=\xi_0} = \frac{\sinh\xi_0}{\sqrt{\sinh^2\xi_0+\sin^2\eta}}\left[\sin^2(\eta)+\frac{4\tanh\xi_0}{\pi}\sum_{n=1}^{\infty}\frac{\coth(2n-1)\xi_0\ \sin(2n-1)\eta}{(2k-3)(2k+1)}\right] \tag{105}$$

$$\tau_{\xi,z}\Big|_{\xi=0} = -\frac{4\cosh\xi_0\tanh^2\xi_0}{\pi\sin\eta}\sum_{n=1}^{\infty}\frac{\sin(2n-1)\eta}{(2k-3)(2k+1)\sinh(2k-1)\xi_0} \tag{106}$$

$$\tau_{\eta,z}\Big|_{\eta=0,\pi} = -\frac{4\cosh\xi_0\ \tanh^2\xi_0}{\pi\sinh\xi}\sum_{n=1}^{\infty}\frac{\sinh(2n-1)\xi}{(2k-3)(2k+1)\sinh(2n-1)\xi_0} \tag{107}$$

Figure 24 shows the distribution of the shear stress around a channel with $b/a = 3/4$. The maximum shear stress acts on the middle of the channel, as expected.

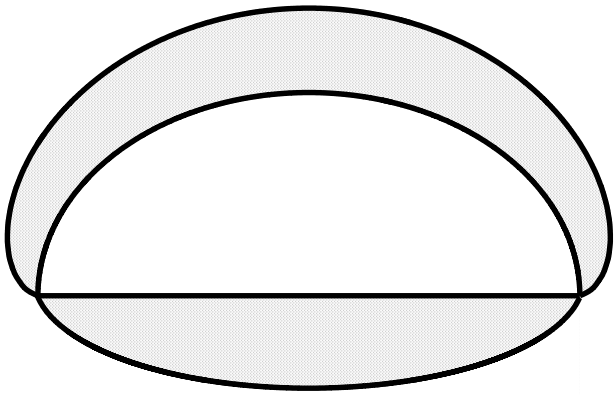

Figure 24: Shear stress for the case $b/a = 3/4$

3.6.5 Average shear stress

The average dimensionless shear stress around the channel can be obtained by averaging the dimensionless shear stress over the perimeter of the cross-section of the channel, ℓ. The perimeter of the channel is calculated by

$$\ell = 2a + \int_0^{\pi} h_\eta\, d\eta = 2a\left[1+E\left(1-(b/a)^2\right)\right] \tag{108}$$

where $E(k) = \int_0^{\pi/2} \sqrt{1 - k \sin^2 \eta}\, d\eta$ is the complete elliptic integral of the second kind.

The average shear stress can, then, be calculated as

$$\bar{\tau} = \frac{\int_{\ell} \tau d\ell}{\ell} = \frac{\pi \ b / a}{4\left[1 + E\left(1 - (b/a)^2\right)\right]} \tag{109}$$

The average shear stress is a function of the axis ratio b/a. It ranges from zero when $b/a = 0$ to a maximum value of $\frac{\pi}{4+2\pi}$ when the channel is semicircular i.e. $b/a = 1$, **Figure 25**.

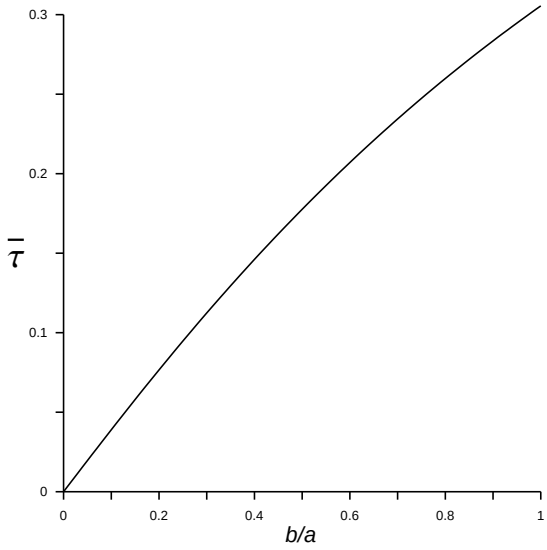

Figure 25: Average shear stress

It is worth noting that expression (109) can be obtained from a simple balance of forces on a segment of length *L* of the channel. Balancing the shear stress against the pressure, **Figure 19(a)**, one can write

$$\bar{\sigma}\ell L = A\Delta P \tag{110}$$

where $\bar{\sigma}$ is the dimensional average shear stress, and ΔP is the pressure drop over the segment of the channel of length L. Equation (109), upon using the expressions for the area and the perimeter in (110), follows immediately.

3.6.6 Comparison with two known approximate expressions

Most of the solutions of the flow through channels with non-classical cross-sections available are only approximate. The most important of such solutions are those by Bahrami et al. [18], and Mortensen et al. [25].

3.6.6.1 Mortensen's result

Mortensen et al. [25] considered pressure-driven, steady-state Poiseuille flow in straight channels with various cross-sectional shapes: elliptic, rectangular, triangular, and harmonic-perturbed circles. The perimeter ℓ and area A which characterize a given shape are combined into the dimensionless **compactness** number given by

$$\mathbb{C} = \ell^2 / A \tag{111}$$

It was found that the hydraulic resistance is characterized by a dimensionless geometrical **correction factor** α. The relation between the correction factor and the compactness is "close-to-linear", which points out $\mathbb{C}$ as a single dimensionless measure characterizing flow properties. It was observed that the **hydraulic resistance** of a channel, R^*_{hyd},

obtained from dimensional analysis does not incorporate the perimeter of the channel, in other words,

$$R^*_{hyd} = \mu L / A^2 \tag{112}$$

This R^*_{hyd} is different from the actually used hydraulic resistance,

$$R_{hyd} = \Delta P / Q \tag{113}$$

where $Q = \int w \, dA$ is the discharge.

Therefore, a geometric correction factor was defined as

$$\alpha = R_{hyd} / R^*_{hyd} \tag{114}$$

Testing several cross-sections, Montensen et al. found that a close-to-linear relationship exists between the geometric correction factor and a compactness number, $\mathbb{C}$.

Consequently, the actual hydraulic resistance is linearly related to that from dimensional analysis. Using Mortensn approach, for semi-elliptic channels, one can show that

$$Q = \frac{-a^2}{\mu}\frac{dP}{dz}\int u \, dA = \frac{-a^2}{\mu}\frac{dP}{dz} A\bar{u} \tag{115}$$

$$R_{hyd} = \frac{\mu L}{a^2 A \bar{u}} \tag{116}$$

$$R^*_{hyd} = \frac{\mu \ell}{A^2} \tag{117}$$

$$\alpha = \frac{\pi}{2\bar{u}}\frac{b}{a} \tag{118}$$

and $\mathbb{C} = \frac{8}{\pi}\frac{1}{b/a}\left[1 + E\left(1 - (b/a)^2\right)\right]^2$ (119)

The parametric plot, **Figure 26**, shows that α and $\mathbb{C}$ are, indeed, linearly close. A fitted linear equation, then, is

$$\alpha \approx \frac{5}{2}\mathbb{C} - 8 \tag{120}$$

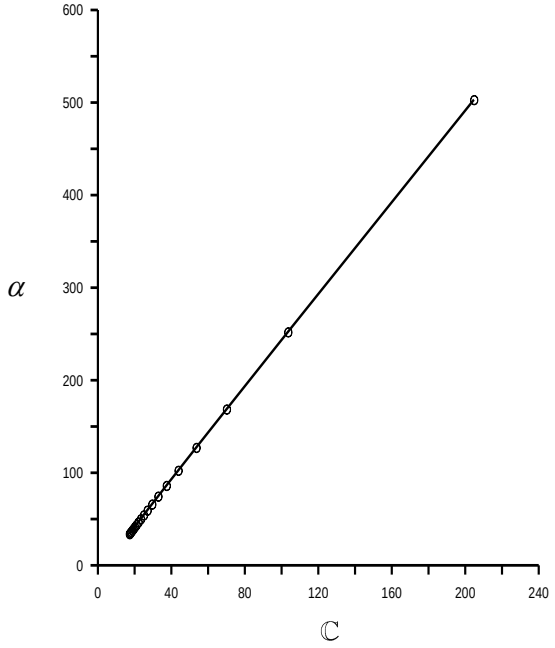

Figure 26: Parametric plot of α v.s. $\mathbb{C}$

3.6.6.2 Bahrami's results

Bahrami et al. [18]0 offers a novel approximate solution for determining the pressure drop of fully developed, laminar, single-phase flow in singly connected microchannels of arbitrary cross-section. Using a ‘‘bottom-up" approach, it was shown that for constant fluid properties and flow rate in fixed cross-section channels, the Poiseuille number is only a function of geometrical parameters of the cross-section, i.e., perimeter, area, and polar moment of inertia. The model is compared against numerical results for a wide variety of channel cross-sections including: hyperellipse, trapezoid, sine, square duct with

two adjacent round corners, rhombic, circular sector, circular segment, annular sector, rectangular with semi-circular ends, and moon-shaped channels.

Following Bahrami et al., the definition of the Fanning friction factor, f, is

$$f = \frac{2\bar{\sigma}}{\rho \bar{w}^2} \tag{121}$$

where $\bar{w}$ is the average dimensional velocity, and ρ is the fluid density. The definition of the **Reynolds number**, $\mathrm{Re}_{\sqrt{A}}$, based on the square root of the area as the characteristic length, is

$$\mathrm{Re}_{\sqrt{A}} = \frac{\rho \bar{w} \sqrt{A}}{\mu} \tag{122}$$

Bahrami et al. showed that the square root of the cross-sectional area, as characteristic length, is superior to the conventional hydraulic diameter in the sense that it leads to similar trends in the values of the dimensionless friction factors for channels with different cross-sections. The product of Fanning friction factor and Reynolds number reduces to

$$f\ \mathrm{Re}_{\sqrt{A}} = \frac{\left(\frac{\pi}{2}\frac{b}{a}\right)^{3/2}}{\left[1+E\left(1-\left(\frac{b}{a}\right)^2\right)\right]\bar{u}} \tag{123}$$

It was observed by Bahrami et al. that torsion in beams and fully developed laminar flow in ducts are similar in the sense that the governing equation for both problems is Poisson's equation. Using the concept of Saint-Venant of approximating the torsional

rigidity of a shaft, Bahrami et al. proposes the following approximate formula for the product of Fanning friction factor and Reynolds number for channels of arbitrary cross-sections.

$$\left(f\ \mathrm{Re}_{\sqrt{A}}\right)_{\text{Bahrami}} = 32\pi^2 \frac{I_P}{A^2} \frac{\sqrt{A}}{\ell} \tag{124}$$

where I_P is the polar moment of inertia defined as

$$I_P = \int_A \int \left[\left(x - \bar{x}\right)^2 + \left(y - \bar{y}\right)^2 \right] dA \tag{125}$$

where $\bar{x}$ and $\bar{y}$ are the coordinates of the "center of mass" of the cross-section. For a semi-elliptic channel, it is easy to see that $\bar{x}$, measured from the center of the channel, is

$$\bar{x} = 0 \tag{126}$$

and $\bar{y}$, measured from the bottom of the channel, is

$$\bar{y} = \frac{\int y\, dA}{A} = \frac{4b}{3\pi} \tag{127}$$

The polar moment of inertia, then, can be calculated as

$$I_P = \frac{ab\left[9\pi^2 a^2 + 9\pi^2 b^2 - 64b^2\right]}{72\pi} \tag{128}$$

Equation (124), then, can be written for semi-elliptic cross-section as

$$\left(f\ \mathrm{Re}_{\sqrt{A}}\right)_{\text{Bahrami}} = \frac{8}{9} \frac{1}{\sqrt{2\pi\left(b/a\right)}} \frac{\left[\left(9\pi^2 - 64\right)\left(b/a\right)^2 + 9\pi^2\right]}{\left[1 + E\left(1 - \left(b/a\right)^2\right)\right]} \tag{129}$$

Figure 27 shows the comparison between the exact expression (123) against the approximate expression (129). The figure shows that the approximate expression of Bahrami et al. is, indeed, an excellent one. The maximum difference between the two expressions is 3% when $b/a = 1$.

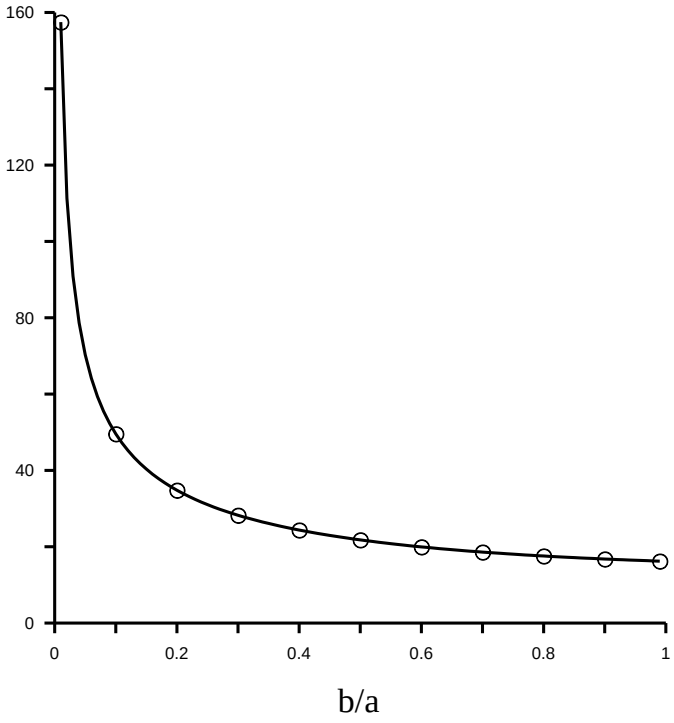

Figure 27: Exact $f\ \mathrm{Re}_{\sqrt{A}}$ (solid line) v.s. Bahrami's approximate expression (circles).

CHAPTER 4: Heat Conduction from a Tours

4.1 Introduction

Several industries involve cooling of ring-like blanks (donuts),

Figure 28. In such industries, which are not limited to food processing, it is very important to estimate, for example, the cooling time of such products before packaging, [26].

Production/Fabrication Cooling Packing

Figure 28: Typical production process

4.2 Problem Statement

The problem considered here is that of a ring torus (donut) with inner radius r and outer radius R, at a uniform temperature T_s in a medium of constant temperature T_f, **Figure 29**. It is desired to find the thermal field in the region outside the tours.

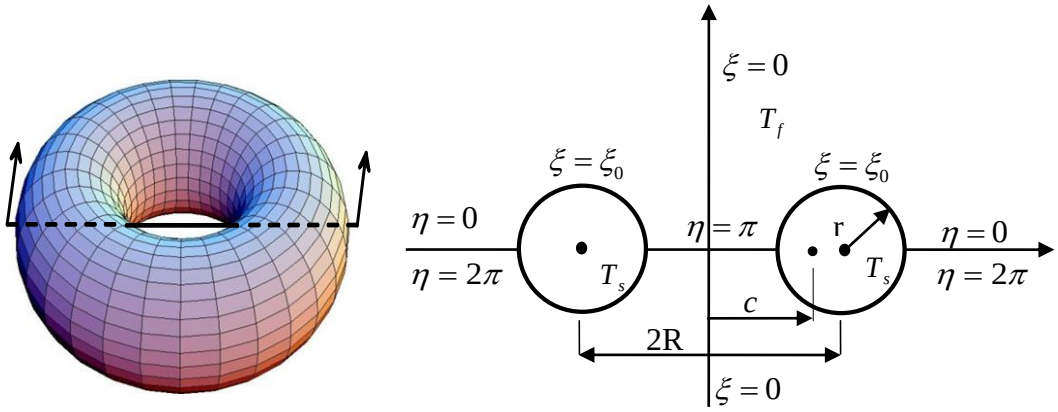

Figure 29: Problem configuration

4.3 Toroidal Coordinates System

A torus is generated by revolving a circle in three dimensional space about a coplanar axis which does not necessarily touch the circle. If the axis touches the circle, the resulting surface is a horn torus. Furthermore, if the axis is a chord of the circle, the resulting surface is a spindle torus, **Figure 30**. A sphere is generated at the case when the axis is a diameter of the circle, [1, 2, 3].

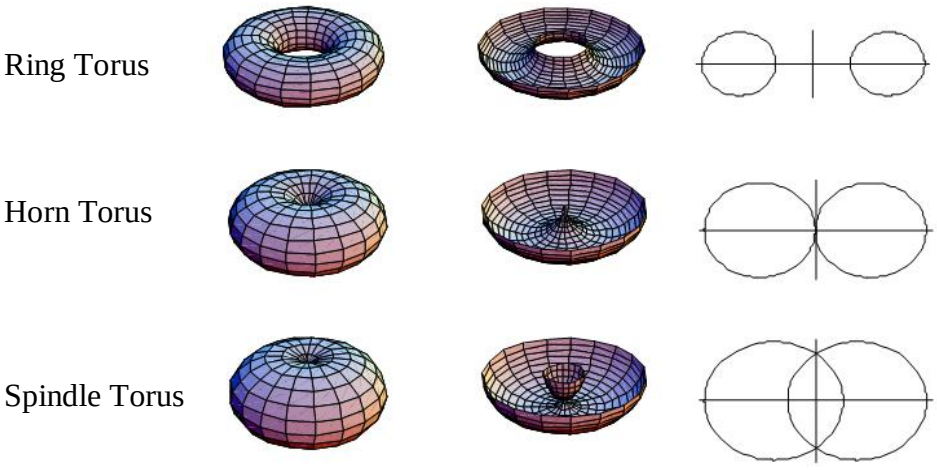

Figure 30: Standard Toroids

To suit the geometry of the problem, the toroidal coordinates system (η,ξ,ϕ) is used. This system is related to the cartesian coordinates system by the relations

$$\begin{aligned} x &= \frac{c\ \sinh\xi\ \cos\phi}{\cosh\xi-\cos\eta} \\ y &= \frac{c\ \sinh\xi\ \sin\phi}{\cosh\xi-\cos\eta} \\ z &= \frac{c\ \sin\eta}{\cosh\xi-\cos\eta} \end{aligned} \tag{130}$$

where $(0\le\xi<\infty)$, $(0\le\eta<2\pi)$, and $(0\le\phi<2\pi)$ and $c=\sqrt{R^2-r^2}$ is the focal distance. The corresponding scale factors are given by

$$h_\eta = h_\xi = \frac{c}{\cosh\xi-\cos\eta}, \qquad h_\phi = \frac{c\ \sinh\xi}{\cosh\xi-\cos\eta} \tag{131}$$

The toroidal coordinates system, **Figure 31**, is composed of the following coordinate surfaces:

- Spherical bowls, ($\eta=\text{constant}$), $x^2+y^2+(z-c\ \cot\eta)^2=c^2/\sin^2\eta$
- Toroids ($\xi=\text{constant}$), $x^2+y^2+z^2+c^2=2c\sqrt{x^2+y^2}\coth\xi$
- Half planes through the *z*-axis, ($\phi=\text{constant}$), $y=x\ \tan\phi$

An infinitesimal volume element in toroidal coordinates system is given by

$$dV = h_\eta h_\xi h_\phi\, d\eta\, d\xi\, d\phi = \frac{c^3\ \sinh\xi}{(\cosh\xi-\cos\eta)^3} \tag{132}$$

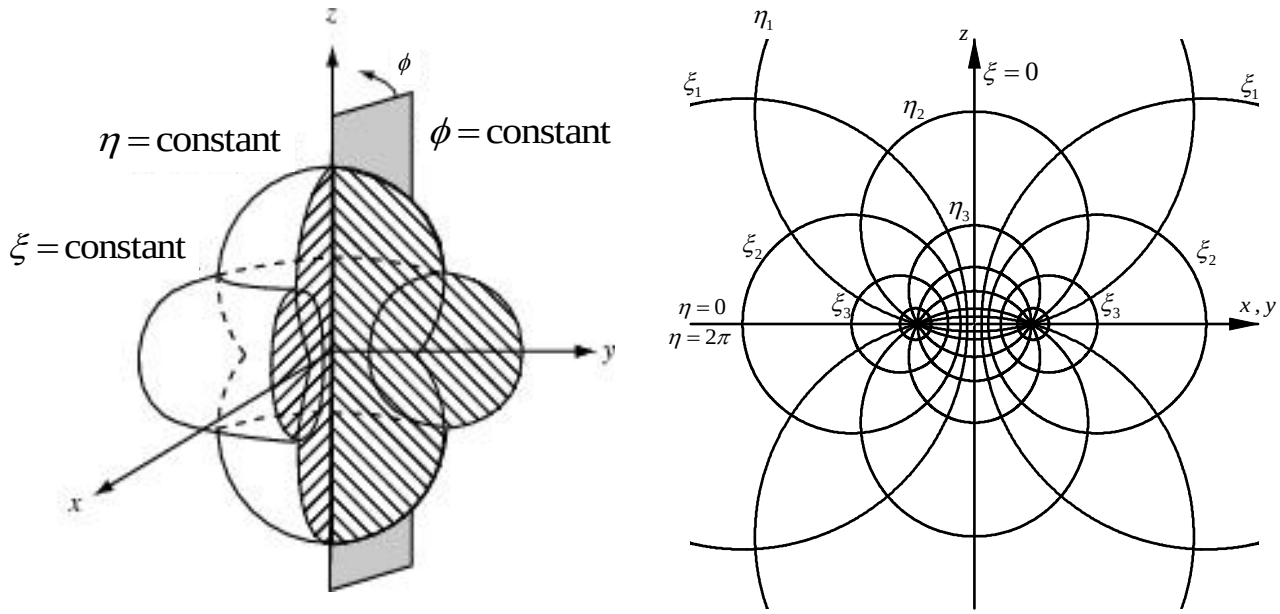

Figure 31: Toroidal Coordinates, [29]

The outer surface of the tours is defined by ξ_0 which is related to the radii ratio R / r by

$$\xi_0 = \cosh^{-1}\left(\frac{R}{r}\right) \tag{133}$$

The point $(\eta, \xi) \to (0,0)$ defines the far field away from the torus where the temperature is T_f .

4.4 Governing Differential Equation and Boundary Conditions

Using the scale factors (131) in equation (30), the steady state heat equation specialized for toroidal coordinates may be written as

$$\frac{\partial}{\partial \xi}\left(\frac{\sinh \xi}{\cosh \xi - \cos \eta}\frac{\partial T}{\partial \xi}\right) + \frac{\partial}{\partial \eta}\left(\frac{\sinh \xi}{\cosh \xi - \cos \eta}\frac{\partial T}{\partial \eta}\right) = 0 \tag{134}$$

The boundary conditions to be satisfied are

$$T(\eta,\xi_0)=T_s, \qquad T\big|_{(\eta,\xi)\to(0,0)}=T_f \tag{135}$$

The first boundary condition corresponds to the case where the surface of the torus is maintained at constant temperature (that of the infinite medium and is well justified for high Biot numbers). This condition may be easily modified to accommodate cases of low Biot numbers. The second condition accommodates only bounded solutions inside the torus.

4.5 Series Expansion Solution

Define the dimensionless temperature as

$$u(\eta,\xi)=\frac{T-T_f}{T_s-T_f} \tag{136}$$

Equation (134) and the conditions (135) can now be rewritten in terms of the dimensionless temperature as

$$\frac{\partial}{\partial\xi}\left(\frac{\sinh\xi}{\cosh\xi-\cos\eta}\frac{\partial u}{\partial\xi}\right)+\frac{\partial}{\partial\eta}\left(\frac{\sinh\xi}{\cosh\xi-\cos\eta}\frac{\partial u}{\partial\eta}\right)=0 \tag{137}$$

$$u(\eta,\xi_0)=1, \qquad u\big|_{(\eta,\xi)\to(0,0)}=0 \tag{138}$$

The energy equation (137) is R-separable in toroidal coordinates. Therefore, one can assume a solution of the form

$$u(\eta,\xi)\equiv\sqrt{\cosh\xi-\cos\eta}\,X(\xi)\,Y(\eta) \tag{139}$$

Upon substituting (139) in (137), and performing the necessary rituals, one finds that the basis functions are $P_{n-\frac{1}{2}}(\cosh\xi)$, $Q_{n-\frac{1}{2}}(\cosh\xi)$, $\cos n\eta$, and $\sin n\eta$, where $P_{n-\frac{1}{2}}$ and $Q_{n-\frac{1}{2}}$ are the toroidal functions of the first and second kinds respectively. Due to the boundary conditions in (138) and the boundedness requirements, only $P_{n-\frac{1}{2}}$ and $\cos n\eta$ survive. The solution can then be written as

$$u(\eta,\xi)=\sqrt{\cosh\xi-\cos\eta}\sum_{n=0}^{\infty}A_n P_{n-\frac{1}{2}}(\cosh\xi)\cos(n\eta) \tag{140}$$

Applying the first condition in (138), in addition to the integral, [28]0,

$$\int_0^{2\pi}\frac{\cos(n\eta)}{\sqrt{\cosh\xi-\cos\eta}}d\eta=2\sqrt{2}\,Q_{n-\frac{1}{2}}(\cosh\xi) \tag{141}$$

the expression of A_n can be found as

$$A_n=\frac{2\sqrt{2}}{\pi(1+\delta_{n0})}\frac{Q_{n-\frac{1}{2}}(\cosh\xi_0)}{P_{n-\frac{1}{2}}(\cosh\xi_0)} \tag{142}$$

Thus, the complete solution of (137) is

$$u(\eta,\xi)=\sqrt{\cosh\xi-\cos\eta}\sum_{n=0}^{\infty}\frac{2\sqrt{2}}{\pi(1+\delta_{n0})}\frac{Q_{n-\frac{1}{2}}(\cosh\xi_0)}{P_{n-\frac{1}{2}}(\cosh\xi_0)}P_{n-\frac{1}{2}}(\cosh\xi)\cos(n\eta) \tag{143}$$

Contour plots of the solution (143) for $r = 1$ and $R = 3/2, 5/2, \text{and } 7/2$ are shown in **Figure 32**.

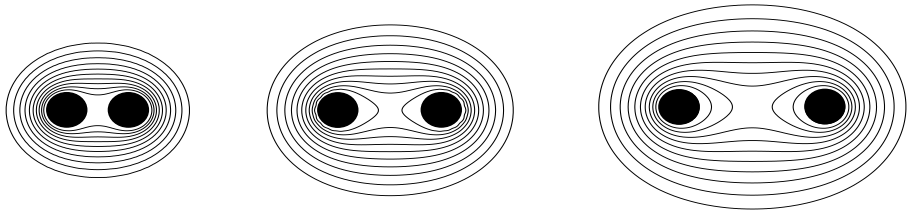

Figure 32: Dimensionless temperature distribution for the cases $r = 1$ and $R = 3/2, 5/2, \text{and } 7/2$

Conclusion

In this research, general simple expressions for the curl and divergence operators in general curvilinear coordinates, whether orthogonal or skew, have been derived. These expressions appear in the governing equations of several physical systems. Three problems related to heat transfer and fluid flow are of interest and have been dealt with in the present study. These are:

***Conduction in a Spheroid*:** Two different solutions of the transient heat conduction in a hot spheroid (oblate or prolate) left to cool in a medium of fixed temperature have been obtained. The first solution, upon recasting the governing equations in spheroidal coordinates, makes use of the spheroidal wave functions as basis for a series expansion. The second is numerical where the temperature is expanded in terms of Legendre functions. An implicit finite difference scheme is, then, implemented to obtain the time development of the thermal field. The two solutions have been compared and further verified against the solution for the limiting case of a perfect sphere. The effect of the axis ratio on the time development of the temperature inside the spheroid and the heat transfer rate across the surface has been studied.

Hagen-Poiseuille Flow in a Tube of Semi-Elliptic Cross Section: A solution for Hagen-Poiseuille flow in a tube of semi-elliptic cross section has been obtained. As a natural host, the governing equation is dealt with in elliptic cylindrical coordinates. The solution has been verified by comparing it with the limiting case of a semi-circular cross-

section in addition to two known approximate solutions. The average and maximum velocities have been determined in addition to the shear stress distribution along the wall of the channel. The effect of the circularity of the channel has also been studied.

Conduction from a Torus: The steady state equation of heat transfer from a constant temperature torus in an unbounded medium was written in toroidal coordinates. An exact solution of the thermal field outside the torus has been obtained.

References

[1] G. Arfken, Mathematical Methods for Physicists, 3rd ed. Orlando, FL: Academic Press, 1985.

[2] P. Moon, and D.E. Spencer, Field Theory for Engineers. Princeton, NJ: Van Nostrand, 1961.

[3] P.M. Morse, and H. Feshbach, Methods of Theoretical Physics, Part I. New York: McGraw-Hill, 1953.

[4] M. M. R. Williams, Thermophoretic forces acting on a spheroid, J. Phys. D.: Appl. Phys. 19, pp. 1631-1642, 1986.

[5] C. Niven, On the conduction of heat in ellipsoids of revolution, Phil. Trans. Roy. Soc. London, 171: 117-151, 1880.

[6] P.E. Falloon, P.C. Abbott, and J.B. Wang, Theory and Computation of the Spheroidal Wave Functions, Journal of physics. A, mathematical and general, vol. 36, no. 20, pp. 5477-5495, 2003.

[7] C. Flammer, Spheroidal Wave Functions, Stanford Univ. Press, Stanford, CA, 1957.

[8] M. Abramowitz and I. A. Stegun, Handbook of Mathematical Functions, 9th ed. New York: Dover, 1970.

[9] J. A. Stratton, Electromagnetic Theory. New York: McGraw-Hill, 1941.

[10] J. Meixner, F.W. Schäfke, G. Wolf, in: A. Dold, B. Eckmann (Eds.), Mathieu Functions and Spheroidal Functions and Their Mathematical Foundations, Further Studies, in: Lecture Notes in Math., Vol. 837, Springer-Verlag, New York, NY, 1980.

[11] J. Caldwell, Computation of eigenvalues of spheroidal harmonics using relaxation, Journal of Physica A-Mathematical and General, volume 21, Issue 19, pp. 3685-3693, 1988.

[12] D.B. Hodge, Eigenvalues and eigenfunctions of spheroidal wave equation, Journal of Mathematical Physics, volume 11, Issue 8, pp. 2308-&, 19970.

[13] L. Baker, C. Mathematical Function Handbook, McGraw Hill, New York, 1992.

[14] L.W. Li, X.K. Kang, and M.S. Leong, Spheroidal wave functions in electromagnetic theory, Wiley, 2002.

[15] A.I. Zayed, A generalization of the prolate spheroidal wave functions, Proceedings of the American Mathematical Society, volume 135, no. 7, pp. 2193–2203, 2007.

[16] D. J. Ivers, An angular spectral method of the solution of the heat equation in spheroidal geometries, ANZIAM J. 46 (E), pp. C854-C870, 2005.

[17] R.S. Alassar, Heat conduction from spheroids, ASME Journal of Heat Transfer, vol. 121, pp. 497-499, 1999.

[18] Bahrami, M., Michael Yovanovich, M., and Richard Culham, J., A novel solution for pressure drop in singly connected microchannels of arbitrary cross-section. International Journal of Heat and Mass Transfer, 2007. 50(13-14): p. 2492-2502.

[19] T. Minamitani, T. Hayashi, K. Hasegawa, and Y. Kikuchi, Micro-Channel Flow Analyzers for Visualization of Micro-fluidic Simulations, Proceedings of the 26th Annual International Conference of the IEEE EMBS, San Francisco, CA, USA • September 1-5, 2004.

[20] Gou-JenWang, Cheng-Chih Hsueh, Shan-hui Hsu, and Huey-Shan Hung, Fabrication of PLGA microvessel scaffolds with circular microchannels using soft lithography, J. Micromech. Microeng. 17 (2007) 2000–2005.

[21] Ziaie, B., Baldi, A., Lei, M., Gu, Y., and Siegel, R.A., Hard and soft micromachining for BioMEMS: review of techniques and examples of applications in microfluidics and drug delivery. Advanced Drug Delivery Reviews, 2004. 56(2): p. 145-172.

[22] Chang-Yi Wang, Ying-Hong Liu, and Chien C. Chang, Analytical solution of electro-osmotic flow in a semicircular microchannel, Physics of Fluids, 20, (2008), 063105.

[23] Zhipeng Duan, and Y. S. Muzychka, Slip flow in non-circular microchannels, Microfluid Nanofluid (2007) 3:473–484.

[24] Babak Ziaiea,b, Antonio Baldia, Ming Leia, Yuandong Guc, Ronald A. Siegel, Hard and soft micromachining for BioMEMS: review of techniques and examples of applications in microfluidics and drug delivery, Advanced Drug Delivery Reviews 56 (2004) 145– 172.

[25] Mortensen, N.A., Okkels, F., and Bruus, H., Reexamination of Hagen-Poiseuille flow: Shape dependence of the hydraulic resistance in microchannels. Physical Review E, 2005. 71(5): p. 057301.

[26] Wiesche, S. A., Transient Heat Conduction in a Torus: Theory and Application, HMT, 38, 85-92, 2001.

[27] Andrews, M., Alternative Separation of Laplace's Equation in Toroidal Coordinates and its Application to Electrostatics, Journal of Electrostatics, 64, 664-672, 2006.

[28] Gradshteyn, I.S. and Riyzhik, I.M., Tables of Integrals, Series and Products, Fourth (English) Edition, (Prepared by Alan Jeffrey), Academic Press, New York, 1980.

[29] Http://www.wolframalpha.com/

Vita

Name: Mohammed Ahmed AbuShoshah

Nationality: Saudi

Date of Birth: 8/3/1408 - 31/10/1987

Email: M.Shusha@gmail.com

Mobile: (+966) 504 677 929

Academic Background

B.S. degree in Electrical Engineering from King Fahd University of Petroleum and Minerals, KFUPM, June 2010.